

Lateral, polycentric flow of the Nandurbar-Dhule Deccan dyke swarm inferred from magnetic fabric analysis: Evidence of ‘fissure-fed’ volcanism

Ayanangshu Das¹ and Jyotirmoy Mallik¹

¹IISER Bhopal

November 24, 2022

Abstract

The emplacement mechanism of the Deccan province in India had been argued by researchers to a great extent. One of the most favoured hypotheses is “” facilitated by major pre or syn-Deccan crustal extension i.e. the Deccan flood basalts are dyke fed. Determination of flow direction, not only provides indirect evidence in proving or disproving the hypothesis, it also provides clues on its association with a mantle plume, depth of the feeder chambers, etc. In this paper, we have studied Nandurbar-Dhule (DND) Deccan dyke swarm (~210 mappable dykes) from Western India, that intruded compound basaltic (older than dykes) lava flows. Multiple oriented samples were collected from fourteen dykes of the swarm and their magnetic fabrics were delineated by Anisotropy of Magnetic Susceptibility (AMS) technique. The study was complemented by petrography and rock magnetic analysis to decipher the magnetic mineralogy and domain structure. AMS analysis suggests that most of the studied dykes display inclined/lateral flows which are likely in most large dyke swarms. Moreover, the cumulative flow geometry suggests the dominance of polycentric flow i.e. there were multiple magma sources and there were no preferable flow direction. Our results are strongly in line with the geochemical and isotopic signatures (that also establishes lateral, polycentric flow and indicates that the dykes are feeders to the younger Deccan flow) found independently by other groups of researchers. Finally, we discuss the merit of “eruption through fissures” hypothesis and its likely association with a mantle plume in the light of our results.

**Lateral, polycentric flow of the Nandurbar-Dhule Deccan dyke swarm
inferred from magnetic fabric analysis: Evidence of ‘fissure-fed’ volcanism**

Ayanangshu Das^a and Jyotirmoy Mallik^{*b}

^a Ph.D. student, Department of Earth and Environmental Sciences, Indian Institute of Science Education and Research Bhopal, Madhya Pradesh, India-462066.

^{*b} Corresponding author: Assistant Professor, Department of Earth and Environmental Sciences, Indian Institute of Science Education and Research Bhopal, Madhya Pradesh, India-462066. (*E-mail: jmallik@iiserb.ac.in, Voice: 7044133014)

1 **Lateral, polycentric flow of the Nandurbar-Dhule Deccan dyke swarm**
2 **inferred from magnetic fabric analysis: Evidence of ‘fissure-fed’ volcanism**

3
4 **Ayanangshu Das^a and Jyotirmoy Mallik^{*b}**

5
6 **Abstract:**

7 The emplacement mechanism of the Deccan province in India had been argued by
8 researchers to a great extent. One of the most favoured hypotheses is “*eruption through*
9 *fissures*” facilitated by major pre or syn-Deccan crustal extension i.e. the Deccan flood
10 basalts are dyke fed. Determination of flow direction, not only provides indirect evidence in
11 proving or disproving the hypothesis, it also provides clues on its association with a mantle
12 plume, depth of the feeder chambers, etc. In this paper, we have studied Nandurbar-Dhule
13 (DND) Deccan dyke swarm (~210 mappable dykes) from Western India, that intruded
14 compound basaltic (older than dykes) lava flows. Multiple oriented samples were collected
15 from fourteen dykes of the swarm and their magnetic fabrics were delineated by Anisotropy
16 of Magnetic Susceptibility (AMS) technique. The study was complemented by petrography
17 and rock magnetic analysis to decipher the magnetic mineralogy and domain structure. AMS
18 analysis suggests that most of the studied dykes display inclined/lateral flows which are
19 likely in most large dyke swarms. Moreover, the cumulative flow geometry suggests the
20 dominance of polycentric flow i.e. there were multiple magma sources and there were no
21 preferable flow direction. Our results are strongly in line with the geochemical and isotopic
22 signatures (that also establishes lateral, polycentric flow and indicates that the dykes are
23 feeders to the younger Deccan flow) found independently by other groups of researchers.
24 Finally, we discuss the merit of “eruption through fissures” hypothesis and its likely
25 association with a mantle plume in the light of our results.

26 **Key words:** Dyke, AMS, Emplacement, Deccan, polycentric flow.

27 **1. Introduction:**

28 The understanding of complex manoeuvres of magma in the crust provides remarkable
29 insights into the dynamic processes governing the feeder systems for any volcanic eruptions
30 (e.g., Curtis et al., 2008; Magee et al., 2018; Pan et al., 2014; Tibaldi, 2015). On being pushed
31 into the crust, magmatic fluids may get stored into reservoirs at various depths and pass
32 through the crust forming intrusions like dykes, inclined sheets, and sills (e.g., Martin et al.,
33 2019; Mathieu et al., 2008).

34 The magma movement can be vertical from a deeper source directly to the surface or a
35 shallower chamber or the movement can be lateral away from the source and spread over a
36 large area (Pan et al., 2014). Such movements could be related to larger mantle plumes (Ernst
37 and Baragar, 1992) or smaller localized sources (Archanjo et al., 2000). Depending on the
38 type of movement and dyke geometry, injection type can be indicated; whether it is a product
39 of passive injection (Pan et al., 2014) or injected under a radial stress field associated with a
40 mantle plume (Curtis et al., 2008) or emplaced through existing faults and fractures or
41 emplaced passively under strong anisotropic horizontal stresses.

42 Traditional techniques of magma flow fabric determination using petrographic features such
43 as complex forking directions, cryptic layering in composite dykes, vesicle orientations,
44 xenolith alignment etc. (Pan et al., 2014; Philpotts and Asher, 1994) and field evidences (viz:
45 primary foliation and lineation governed by fluid flow) make it a cumbersome task to
46 envisage the entire magma dynamics through the dykes. Besides, the association of a large
47 number of dykes with most of the CFB's causes added inconveniences. Hence, Graham
48 (1954) came up with the idea of using Anisotropy of Magnetic Susceptibility (AMS)
49 technique to detect petrofabric preserved in rock samples. Using AMS, the orientation of
50 three susceptibility axes (k_1 , k_2 , and k_3) are measured to reconstruct the shape and orientation
51 of the magnetic fabric. From this fabric orientation, a sense of magma flow and its direction

52 can be determined. This method has already been tried and tested a lot of time to investigate
53 flow direction and flow-induced strain in mafic rocks (e.g., Kodama, 1995; MacDonald and
54 Ellwood, 1987; Martín-Hernández et al., 2004; Ort et al., 2015; Rochette et al., 1992; Tarling
55 and Hrouda, 1993). Knight and Walker (1988) and Ernst (1990) first applied the AMS
56 technique to Proterozoic mafic dyke swarms as a proxy to primary magmatic flow directions.
57 Since then, AMS technique has become an efficient and time-saving tool in understanding the
58 emplacement mechanism of dyke swarms in different tectonic frames, viz: Hawaiian dykes
59 (Knight and Walker, 1988), the Troodos ophiolite (Staudigel et al., 1992), Makhtesh Ramon
60 dykes, Israel (Baer, 1995), the Independence dyke swarm, California (Dinter et al., 1996),
61 Cretaceous mafic dykes in the Moyar Shear Zone (MSZ) area (Pratheesh et al., 2011),
62 radiating dyke swarm in the Eastern Dharwar Craton, Southern India (Kumar et al., 2015)
63 and others (see Cañón-Tapia 2004 for a review).

64 The Deccan volcanic province (DVP) of India is one of the classic examples of continental
65 flood basalts in the world. The tholeiitic Deccan volcanics, distributed over an area of
66 5,00,000 km² area, are estimated to make up a lava volume of $\sim(1-3)\times 10^6$ km³ (Sheth et al.,
67 2019; Wadia, 1975; Sen, 2001; Jay et al., 2009). Based on geochemistry, petrography, field
68 evidence, radiometric and magnetostratigraphic ages, DVP has been categorized into three
69 subgroups (viz: Wai, Lonavla and Kalsubai) with three corresponding magnetic reversal
70 episodes viz: 29N ($\sim >65.6$ Ma)-29R ($\sim 65.6-64.8$ Ma)-30N ($\sim <64.8$ Ma) (Beane et al., 1986;
71 Bondre et al., 2004; Brown et al., 2011; Cashman et al., 1999; Chenet et al., 2007, 2008; Cox
72 and Hawkesworth, 1985; Deshmukh, 1988; Devey and Lightfoot, 1986; Duraiswami et al.,
73 2014; Godbole et al., 1996; Jay and Widdowson, 2008; Keller et al., 2008; Keller et al., 2012;
74 Keszthelyi et al., 1999; Renne et al., 2015; Scheone et al., 2015; Subbarao and Hooper, 1988;
75 Vandamme and Courtillot, 1992; Walker, 1969 and 1971). The magnetic chron 29R is
76 speculated to be the period of peak Deccan volcanism straddling the Cretaceous-Tertiary (K-

77 T) boundary (Chenet et al., 2008; Keller et al., 2012). Like all continental flood basalt (CFB)
78 provinces, the DVP is also ornamented with three large dyke swarms: the West coast dyke
79 swarm (N-S trending), the Narmada-Satpura-Tapi (N-S-T) swarm (E-W trending), and
80 'randomly oriented' Pune-Nasik (P-N) swarm (Fig. 1). The Dhule-Nandurbar Deccan (DND)
81 dyke swarm which is a part of the larger N-S-T swarm, consists of ~210 mappable dykes
82 exposed over an area of 14,500 km² intrude the older Deccan flows of the Dhule-Nandurbar
83 area of the state of Maharashtra, western India.

84

85 The arguments involving age and duration of Deccan emplacement have been the area of
86 great scientific interest since a long time. Three models have been speculated which include
87 viz: i) the coupled effect of mantle plume (Reunion hotspot) and late crustal rifting during
88 India's northward expedition (Campbell, 2005; Duncan and Richards, 1991; Ernst and
89 Buchan, 2003; Richards et al., 1989; White and McKenzie, 1989;); ii) the effect of pre-
90 eruption lithospheric extension (Hawkesworth et al., 2000; King and Anderson, 1995; Turner
91 et al., 1996; Sheth, 2005); and iii) the effect of continental rifting and decompression melting
92 due to small scale mantle convection (Sheth, 1999a,b; 2005). This conflicts encourage the
93 deployment of several up to the minute methods like radiometric dating, geochemical
94 mapping, palaeomagnetism etc., (Alexander, 1981; Bakshi, 1987; Balasubrahmanyam and
95 Snelling, 1981; Bhattacharji et al., 2004; Courtillot et al., 1986; Courtillot et al., 2000;
96 Herrero-Bervera et al., 2001; Mahoney, 1988, Paul et al., 2008, Prasad et al., 1996; Sethna et
97 al., 1990; Sheth et al., 2019; Wensink, 1973, Wensink and Klootwijk, 1971) etc. Due to the
98 large volume of Deccan volcanic rocks, it's extensive areal coverage and contradictory
99 scientific signatures, much of the issues are still debated instead of multiple studies been
100 carried out.

101

102 In the present study, fourteen dykes were analysed by using AMS technique (Fig.1) from the
103 DND swarm. The sampling locations cover most of the geographical area where the dykes
104 are exposed. AMS study was complemented with the petrography and Scanning Electron
105 Microscopy (SEM), and Rock-magnetic analysis viz: bulk susceptibility measurements,
106 temperature dependant susceptibility (κ -T) analysis, Isothermal Remanent Magnetisation
107 (IRM) analysis and vibrating spinner magnetometric (VSM) analysis especially for the
108 identification of magnetic minerals and magnetic domain (responsible for magnetic fabric).
109 This step is essential to answer some basic questions like a) can the relationship between
110 shape fabric and AMS be established? Wherever the shape fabric governed by the silicate
111 minerals i.e. the flow fabric agrees with the magnetic fabric, there the AMS data can be used
112 as a proxy for flow fabric. b) is there any single domain effect (SD)? If the multi-domain
113 grains dominate, maximum susceptibility axis (k_1) would indicate the flow direction whereas
114 the dominance of SD or Pseudo-SD grains lead to more complex interpretation matrix which
115 will be discussed in detail) is there any post-emplacement recrystallization of magnetic
116 minerals affecting the AMS results? Post emplacement alterations could have affected the
117 domain state of magnetic particles and the fabric configuration which in turn alter the way of
118 interpretation. Answers to these questions are prerequisites for any comprehensive and
119 meaningful AMS data interpretation. The derived flow geometry helped to comment on depth
120 of the magma chamber, its possible association with mantle plume. Moreover, it provided
121 with evidence in support of the hypothesis of dyke fed volcanism at least for the late stage of
122 Deccan eruption.

123

124

125 **2. Geological Background:**

126 Topographically, DND dyke swarm is situated on a flat region at an altitude of ~200m with
127 respect to the mean sea level. Numerous mafic dykes intruded compound flood basalts
128 belonging to the Deccan Trap in this area. This 870m thick basalt sequence (Fig. 1), bounded
129 by Satpura mountain ranges to the North, is dominated by Compound flows with numerous
130 columnar joints indicating prolonged sub-aerial exposure. Mostly gently dipping (5–10°) lava
131 flows are quite weathered (Fig. 1) around Dhule and Dondaicha area. Linear ridges formed
132 by the erosion-resistant, unaltered dykes run for several kilometres (longest dyke ~54 Km).
133 The occurrence of the dykes is abundant in the Nandurbar area and gets scarcer farther away
134 from this region (Fig. 1). Geochemical-isotopic data from some mafic lava and dykes from
135 the area (e.g., Sheth et al., 1997, 2004; Mahoney et al., 2000) indicate the variable degree of
136 resemblance with lava flows situated in the Western Ghats. They reported higher radiogenic
137 $(^{87}\text{Sr}/^{86}\text{Sr})_t$ and non-radiogenic $(^{143}\text{Nd}/^{144}\text{Nd})_t$ content in DND dykes compared to the Bushe
138 formation (Lonavala sub-group) standard. Moreover, they identified the dyke with highest
139 $(^{87}\text{Sr}/^{86}\text{Sr})_t$ content (~7.2494) till date from DND swarm. Felsic lavas or tuffs are absent, and
140 red beds (altered tuffaceous materials or paleo-weathering profiles) are rare and localized (a
141 few tens of meters in lateral extent; Fig. 2). The dykes show quite consistent trend i.e. ENE-
142 WSW which implies a strongly anisotropic stress condition prevailing during emplacement
143 (Ray et al., 2007). Along the Tapi River, Deccan volcanics are capped by 30-km wide and
144 200–400m thick layer of Tertiary and quaternary alluvium. The base of the lava pile is not
145 exposed, and the lava pile may be a few hundred meters thick. Based upon the geochemical
146 compositions of the DND dykes, it was speculated that the dykes might have been significant
147 contributors to the regional lava stratigraphy which are currently eroded (Ray et al., 2007).
148 Singh (1998) identified an 8-24 km thick igneous layer underlying the DND swarm at ~22
149 Km depth by gravity modelling. He further argued that the base of the igneous layer lies at
150 Moho. Bhattacharjee et al. (2004) performed similar studies and found out that the magma

151 chambers in this region are shallow (depth ranging from 7-8 km). In 1999, based on the MgO
152 content and other geochemical signature, Melluso et al. anticipated the presence of shallow
153 localised magma chamber. Their speculations were later supported by Ray *et al.*, (2007).
154 Sethna et al. (1999) reported at least two distinct episodes of dyke emplacement in this DND
155 dyke swarm based on palaeomagnetic results. They observed that both normal and reversely
156 magnetised dykes from this region intrude the reversely magnetised older flood basalt.
157 Melluso et al. (1999) published mineralogical and whole-rock geochemical data from DND
158 dyke swarm suggesting the presence of relatively shallow magma chambers. According to
159 their data, the dyke composition ranges from basalt to basaltic andesite (~49-54.7% SiO₂)
160 with tholeiitic affinity (Fe₂O₃ ~15%) and falls closer to 1-atm Ol+Plag+Cpx cotectic curve.
161 Mahoney et al. (2000) showed strong similarities in the geochemical and isotopic data from
162 the dykes of DND swarm and neighbouring basalts with that from the Western Ghats. Ray et
163 al. (2007) made an attempt to delineate the tectono-thermal evolution of the flood basalt in
164 this region based on field observations. They argue in favour of a shallow magma chamber
165 feeding the dykes vertically above it and laterally away from it. Ray et al. (2008) reported a
166 high degree of heterogeneity in the Precambrian basement beneath the dyke swarm from the
167 petrographic and geochemical analysis of crustal xenoliths associated with two dykes from
168 this region. From geochemical signatures, they correlate these xenoliths with the Archean
169 Dharwar Craton exposed in the south of the Deccan Volcanic Province (DVP). Prasad et al.
170 (1996) argued for a post-trappean emplacement for DND dyke swarm based on their
171 palaeomagnetic results. Their results suggest a short duration of Deccan volcanism and reject
172 the conjecture about India's northward voyage during that time. Recently Seth et al. (2019)
173 came up with excellent ⁴⁰Ar/³⁹Ar chronometric datasets and proposed an interval of at least
174 ~4.06±0.64/0.68 Myr between 2 dykes situated in DND swarm. In the present study,
175 representative field examples from morphological units depicting dyke occurrences, red bed,

176 felsic xenoliths embedded in dyke units, rarely found second generation dykes cutting
177 through a larger dyke are shown in Fig. 2. The mantle plume model suggests that the DVP
178 came into existence from the “head” of a plume whose “tail” is currently feeding the active
179 reunion island (Morgan, 1981; Richards et al., 1989; Campbell & Griffiths, 1990). Recent
180 researchers (Sheth et al., 2001a; Sheth, 2005a,b; Baksi, 1999, 2005) have strongly argued
181 against this theory and postulated that a non-plume, large scale plate dynamics could have
182 caused the formation of DVP. DVP’s association with major dyke swarms, like the DND
183 dyke swarm parallel to the Proterozoic continental rift zones, aids to the merit of a “fissure
184 fed” volcanism theory contradicting the mantle plume theory.

185

186 **3. Methodology:**

187 Multiple oriented block samples from fourteen dykes were collected for AMS analysis.
188 Special attention was given to collect samples only from the marginal parts of thicker dykes
189 (thickness $\geq 10\text{m}$) as recommended by Das and Mallik (2020). The authors have
190 demonstrated and many others have hinted (Das and Mallik 2020) that the central part of a
191 thick dyke experiences rather slow cooling, resulting loss of shape anisotropy in the
192 magnetite grains and resulting AMS fabric could be completely independent of the flow
193 fabric. Also, the convection and associated backflow is not immediately arrested in the
194 central part of a thick dyke resulting in the destruction of flow derived silicate and mimicking
195 oxide templates. Therefore, sampling from the central part of a thick dyke was avoided.
196 Details of the sampling locations are shown in Fig. 1. Multiple cylindrical cores of 22 mm in
197 height and 25.4 mm in diameter were drilled from each oriented sample. Thin sections
198 oriented with respect to dyke trend were prepared from such cores for petrographic, Scanning
199 Electron Microscopic (SEM) and Energy Dispersive Spectroscopic (EDS) analysis.

200

201 **3.1.Petrography:**

202 3.1.1. *Petrographic analysis:* The oriented thin sections are extensively studied under
203 transmitted light microscope, mainly to identify the mineral phases (especially
204 silicate minerals).

205 3.1.2. *SEM/EDS analysis:* Energy Dispersive Spectroscopic (EDS) analysis of the dyke
206 samples was done with the help of a Scanning Electron Microscope (SEM) mainly
207 to identify the constituent magnetic minerals responsible for the magnetic fabric.

208 **3.2.Rock magnetic analysis:** Rock magnetic analyses were carried out to identify
209 magnetic mineralogy and to delineate domain structures of the remanence carriers as
210 the interpretation of AMS fabric is significantly dependent on them. .

211 3.2.1. *Susceptibility analysis:* The low-field magnetic susceptibility χ_{lf} normalized with
212 respect to the mass acts as a proxy for the bulk ferromagnetic content. The
213 magnetic susceptibility measurement of the representative dyke samples along six
214 mutually orthogonal directions were carried out at two frequencies (viz. $k_{lf} =$
215 0.465 and $k_{hf} = 4.65$ KHz) using Bartington instrument with MS2B sensor housed
216 at Geology department of Savitribai Phule Pune University, India. The frequency-
217 dependent susceptibility (χ_{fd}) i.e. the difference between low frequency
218 susceptibility and high frequency susceptibility was also calculated and expressed
219 in form of percentage ($\chi_{fd}\%$) to assess the presence of very fine grained magnetic
220 particles across the Superparamagnetic (SP)/Stable single domain (SSD) boundary
221 (Liu et al., 2005). $\chi_{fd} \%$ also acts as a proxy for the alteration (chemical/physical)
222 taken place within the dykes.

223 3.2.2. *Isothermal Remanent Magnetisation (IRM) analysis:* Isothermal Remanent
224 Magnetisation (IRM) analysis was conducted on representative dyke samples
225 under increasing applied fields between 0 to 1000mT. The acquired magnetisation

226 was recorded after each step. Then a reverse field was applied and the similar
227 procedure was followed up to -100mT. ASC impulse magnetizer (ASC Scientific,
228 USA) was used to impart the external magnetic field required for the induction of
229 magnetisation and acquired magnetisation was documented using Molspin spinner
230 magnetometer (Magnetic Measurements, U.K) housed at rock magnetic laboratory
231 of the Geology department in Savitribai Phule University, Pune. The IRM analysis
232 is necessary in order to gauge the concentration and domain size of the constituent
233 ferro and antiferromagnetic minerals by calculating several parameters and ratios
234 (e.g., Liu et al., 2012). The saturation isothermal remanent magnetization (SIRM)
235 was measured at the highest applied field i.e. at 1000 mT. The following
236 parameters are calculated and shown in table 1:

237 Two parameters, hard and soft isothermal remanent magnetization, were
238 calculated to gauge the proportion of antiferromagnetic (ex: Hematite) and multi
239 domain (MD) ferromagnetic mineral (ex: Magnetite, maghemite etc.) respectively
240 (Thompson and Oldfield, 1986; Liu et al., 2012). These two parameters follow:

$$241 \text{ Hard-IRM} = 0.5 \times (\text{SIRM} + \text{IRM}_{-300\text{mT}})$$

$$242 \text{ Soft-IRM} = 0.5 \times (\text{SIRM} - \text{IRM}_{-20\text{mT}})$$

243 To visualize the relative proportion of ferromagnetic particles over
244 antiferromagnetic minerals, the demagnetization parameter S-ratio was calculated
245 (Thompson and Oldfield, 1986; Evans and Heller, 2003; Liu et al., 2012)
246 following the equation:

$$247 \text{ S-ratio} = (\text{IRM}_{-100\text{mT}}/\text{SIRM})$$

248 3.2.3. *κ -T analysis*: Temperature dependent susceptibility (κ -T) analysis was executed
249 on pulverized dyke samples using MFK-1A Kappabridge manufactured by
250 AGICO housed at NGRI, Hyderabad. Magnetic susceptibility was thoroughly

251 measured during the heating and cooling procedure within a temperature interval
252 of 30°C to 600°C. Then required correction of the obtained data was done using
253 the RockMagalyzer 1.1 (Leonhardt, 2006). Finally, susceptibility variation with
254 changing temperature was graphically monitored so that any alteration in
255 magnetic mineral compositions and products formed (if any) due to heating
256 (Speyer 1994) could be identified.

257 3.2.4. *Hysteresis loop and domain structure analysis:* All of the dyke samples were
258 subjected to VSM analysis in order to visualize the hysteresis loops governed by
259 the magnetic phases. At room temperature, Magnetic minerals may be
260 conventionally grouped into magnetically disordered (diamagnetic or
261 paramagnetic) or ordered (ferromagnetic, ferrimagnetic, or antiferromagnetic)
262 phases (e.g., Dunlop and Özdemir, 1997). For para and diamagnetic minerals, the
263 induced magnetization (M) is linearly related to applied field (H) and reversible
264 on removal of H. This magnetically disordered status is flaunted by essentially all
265 the major rock-forming (silicate) minerals and most important accessory minerals.
266 In contrast, the induced magnetisation manifests a nonlinear pattern (and
267 commonly irreversible) with changing applied field for magnetically ordered
268 phases (Ferro and ferromagnetic minerals). The acquired magnetization attains
269 saturation on application of adequately strong applied fields, and even after
270 removal of the field, the magnetic phases are usually left with a remanent
271 magnetisation i.e. M_r . Such properties are typical of iron oxides and iron
272 sulphides.

273 Our samples are mafic in composition and known to be containing ferromagnetic
274 phases like magnetite, titanomagnetite etc. The VSM analysis was carried out on
275 at least one representative samples from each dyke and the analysis was

276 performed using The SQUID VSM instrument housed at IISER Bhopal. After data
277 acquisition, the para and diamagnetic effects were corrected using
278 RockMag analyzer 1.1 (Leonhardt, 2006) followed by the calculation of routine
279 hysteresis parameters viz: Coercivity (H_c), coercive remanence (H_{cr}), saturation
280 magnetisation (M_s), saturation remanent magnetisation (M_{rs}). Finally, a Day plot
281 (Day et al., 1977) was prepared with the obtained data.

282 3.3. *Magnetic fabric study (Anisotropy of magnetic Susceptibility (AMS) analysis):*

283 Measurement of magnetic susceptibility and its anisotropy was carried out using the
284 KLY-4S Spinner Kappabridge manufactured by AGICO (Czech Republic) at the
285 magnetic laboratory of the Department of Geology and Geophysics of Indian Institute
286 of Technology, Kharagpur (IIT Kgp), India. The above mentioned instrument has a
287 sensitivity of 0.03×10^{-6} SI an accuracy of 0.1%. Magnetic susceptibility was
288 measured along different direction to obtain the three principal axes of the magnetic
289 susceptibility fabric, viz. k_1 , k_2 and k_3 (Table 2). Different parameters including mean
290 susceptibility (k_m), magnetic foliation (F), magnetic lineation (L), corrected degree of
291 anisotropy (P_j) and shape parameter (T) were calculated and shown in Table 2. Mean
292 or bulk Susceptibility is simply an arithmetic average i.e. $k_m = (k_1 + k_2 + k_3)/3$. The
293 magnetic foliation (F) represents the ($k_1 - k_2$) plane, whereas the magnetic lineation (L)
294 is basically the attitude of k_1 . P_j is the proxy for the degree of anisotropy exhibited by
295 the shape anisotropic ellipsoid and given by:

296 Corrected degree of magnetic anisotropy, $P_j = \exp \{2[(\ln K_1 - \ln K_m)^2 + (\ln K_2 -$
297 $\ln K_m)^2 + (\ln K_3 - \ln K_m)^2]\}^{1/2}$

298 T governs the shape of the susceptibility ellipsoid, i.e. prolate where $T < 1$ or oblate
299 where $T > 1$ (Tarling and Hrouda, 1993) and can be formulated as:

300 Shape parameter $T = [\{2 \ln(k_2/k_3)\} / \ln(k_1/k_3)] - 1$ (Jelinek 1981).

301 **4. Results:**

302 **4.1. Petrography:** Microscopic studies of rock samples collected from DND dyke swarm
303 have been carried out on at least one sample from each site. The dyke samples vary
304 from fine-grained basalt (e.g. DND1) to moderate grained dolerite (e.g. 1A), and even
305 to coarse-grained gabbro (e.g. 47) from the margin towards the maximum
306 concentration cluster (MCC) of the dyke swam. These rocks are mainly crystalline
307 with a negligible amount of glass present. Overall petrographic features of these
308 aphanitic dyke samples comprise groundmass of elongated plagioclase laths and fine-
309 grained clinopyroxenes together with magnetic minerals composed mainly of Fe-Ti
310 oxides (Fig.3).The plagioclase grains are mostly preferably elongated and the
311 clinopyroxenes are anhedral with poorly defined grain boundary. Their modal
312 percentages vary between 55%- 60% of plagioclase, 30%-35% of clinopyroxene and
313 5%-10% of opaque magnetic mineral grains. Mostly larger grains of plagioclase are
314 present as phenocrysts along with finer grains in groundmass giving rise to the
315 porphyritic texture (e.g. 41).It indicates a difference in cooling rate of the magma at
316 different stages of emplacement. These plagioclase phenocrysts with manifold
317 twinning are embedded in the finer groundmass where plagioclase microlites are
318 partially or completely engulfed (sub-ophitic or ophitic texture) by clinopyroxene
319 (e.g. 1A).

320 **4.2. Scanning electron microscopy:** Under Scanning Electron Microscope (SEM), DND
321 dyke samples exhibit profuse occurrences of Fe-Ti oxides occupying the interstitial
322 spaces between plagioclase and clinopyroxene grains (Fig.4). These Fe-Ti oxides are
323 typically the late-stage product of the crystallization sequence and dispersed in the
324 groundmass as mostly subhedral to euhedral grains. The absence of exsolved ilmenite
325 lamellae indicates that there was no high-temperature deuteric oxidation. The SEM

326 image flaunted in Fig. 4 is typical of all the dyke samples showing a good disparity
327 between bright white coloured titano-magnetite and another matrix component. Das
328 and Mallik (2020) plotted the Fe-Ti concentration on the triangular diagram of Fe-Ti
329 oxides ad show that the magnetic mineral compositions fall around titano-magnetite
330 with various Ti amount. Since lava flow is only 65 million years old, significant
331 alteration causing any interruption in the preservation of the primary magnetic
332 signature is less likely. This fact was confirmed by thin section petrography and SEM
333 analysis. Chemically almost homogenous titano-magnetite shows no evidence of
334 release of either Ti or Fe in the groundmass, and thus no evidence of any fluid
335 modifying the magnetic mineralogy is found.

336 **4.3. Rockmagnetic analysis:**

337 4.3.1. *Susceptibility analysis:* The vital rockmagnetic parameters are listed in Table 1.

338 The mass normalized susceptibility χ_{lf} exhibit a mean value of $\sim 115 \times 10^{-8} \text{m}^3 \text{kg}^{-1}$
339 and a median of $101.35 \text{m}^3 \text{kg}^{-1}$ within an interval ranging from 60.49 to 187.65
340 $\text{m}^3 \text{kg}^{-1}$ (Table 1). These high values ($> 100 \times 10^{-8} \text{m}^3 \text{kg}^{-1}$) are representative of
341 ferromagnetic minerals like magnetite, titanomagnetite etc. All of the frequency
342 dependant susceptibility ($\chi_{fd}\%$) display very lower values (mean $\chi_{fd}\% = 0.36$,
343 median = 0.188) implying the deprivation of ultrafine super paramagnetic (SP)
344 particles (< 0.08 micron) (Dearing et al., 1997) and minimalistic alteration of the
345 dykes as evident from the field observation (Fig. 2).

346 4.3.2. *Isothermal Remanent Magnetisation (IRM) analysis:* IRM acquisition and back-
347 field curves are illustrated in Fig. 5a. Attainment of saturation mostly at ~ 200 mT
348 field through stepwise acquisition of IRM indicates the presence of
349 Titanomagnetite (Patil and Rao, 2002; Patil and Arora, 2003). The coercivity
350 range (15-40 mT) also supports the low-coercive titanomagnetite (Cisowski, 1981;

351 Dankers, 1981; Sharma, 1994, Venkatachalapathy et al., 2009) to be the
352 remanence carrier. The calculated parameters, viz: S-ratio, hard-IRM and soft-
353 IRM etc., are listed in Table 1. S-ratio shows highly negative values restricted
354 within -0.9 to -0.1 which is typical of low coercive titanomagnetite. Fig.5b exhibit
355 the occurrence of very high soft-IRM content compared to Hard-IRM because of
356 the prevalence of titanomagnetite.

357 4.3.3. *Temperature dependent susceptibility (κ -T) analysis:* Temperature dependant
358 variation of susceptibility (κ -T curve) for three representative dyke samples is
359 exhibited in Fig. 6. Magnetisation decreases with increasing temperature. Slight
360 decrease of magnetisation followed by a sharp decrement is observed at a
361 temperature $>350^{\circ}\text{C}$ to up to 600°C . Fig. 6b shows a gentler trend of magnetisation
362 decrement between 400 - 500°C after which a sharp decrease is observed again. The
363 cooling curve follows the heating curve but show much lower values of
364 cumulative susceptibility. This may be because of the loss of total magnetite as a
365 consequence of heating. These κ -T curves depict that Ti rich magnetite is the
366 primary remanence carrier.

367 4.3.4. *Hysteresis loop and domain structure analysis:* Hysteresis loop obtained through
368 VSM analysis reflects the magnetic mineralogical composition and their domain
369 state. All the dyke samples are portraying narrow waisted, reversible loops
370 (Fig.7). This specific style of hysteresis loop is quintessential representative of
371 soft ferromagnetic (titanomagnetite) minerals (Day et al., 1977). The effect of
372 constituent para and diamagnetic phases is clearly evident from the “not attaining
373 plateau” nature of hysteresis loops (Fig. 7a). After removal of these para and
374 diamagnetic influence, it is clear that majority of the samples got saturated at
375 applied field well below 1000mT (Fig. 7b). The shape of this hysteresis loops are

376 quite consistent with our observation from IRM analysis. Different hysteresis
377 parameters (viz: M_{rs}/M_s ; H_{cr}/H_c etc.) are calculated and plotted with the help of
378 Rockmaganalyzer 1.0. Finally the obtained Day plot (Day et al., 1977; Fig. 8)
379 specifies the dominating domain state of the representative dyke samples. Our
380 data detects either low-coercive mineral (MD), or a mixture of low and high
381 coercive phases (PSD). The coercivity shows a wide range starting from 3 to
382 87mT. Amongst our studied samples, ~78.57% dyke samples are dominated by
383 multi-domain phases and ~14.28% are dominated by Pseudo-single domain
384 phases. Rest ~7.14% falls outside any specified domain field and left unresolved.
385 For dyke 31, the data point does not correspond to any specific domain state. This
386 is probably due to high concentration of paramagnetic minerals, slightly mixed
387 magnetic mineralogy and instrumental sensitivity.

388 **4.4. Magnetic fabric study:** AMS measurements were carried out on total 28 samples
389 collected from 14 different dykes. Results from AMS analysis and Stereonet
390 representation of k_1 , k_2 , k_3 attitudes are given in table 2. The entire range of mean
391 susceptibility (k_m) (Min k_m : 16.63×10^{-03} ; Max k_m : 74.53×10^{-03} SI) is presented on a
392 histogram (Fig. 9, Table 2). These high values of bulk susceptibility further confirm
393 the presence of ferromagnetic phase like Titanomagnetite (Knight and Walker, 1988;
394 Hargraves et al., 1991; Rochette et al., 1992). The degrees of anisotropy (P_j ; Jelinek,
395 1981) values are quite low and restricted within the range from 1.006 to 1.074 (Fig.
396 10a). This lower P_j is typical of primary fabric formed during cooling and
397 crystallization (Hrouda, 1982). The k_m - P_j plot shows a consistent linearly correlatable
398 distribution with very less number of outliers (Fig. 10a). This is possibly due to
399 increase in the preferred alignment of magnetic particles with an increasing
400 proportion of magnetic phases. However, the shape parameter hardly depends on the

401 mean bulk susceptibility. So this parameter can be of importance while interpreting
402 rock fabric regardless of the relative proportion of magnetic minerals. The shape
403 parameter (T) shows both positive and negative values thereby implying the
404 occurrence of both prolate and oblate fabric with slight dominance of planar fabric
405 (Fig. 10b). From Fig. 10c, it is evident that magnetic lineation and foliations are more
406 or less equally well developed. Acknowledging the effect of magnetic domain
407 structure on the AMS fabric in mind, we group the resultant AMS fabrics as follows:

- 408 I. Type A: AMS fabric follows the conventional geometrical definition of primary
409 ‘normal’ fabric (i.e. magnetic foliation or k_1 - k_2 plane roughly parallels the dyke
410 plane with k_3 at the pole of the plane) in case of Type A fabric. This fabric is
411 evident in seven (SDPD2b, 7, 52, 53, 5, 21, 31) of our fourteen studied dykes.
412 Both oblate and prolate shapes are detected. Magnetic lineation (k_1) ranges from
413 almost horizontal to almost vertical along three major direction (Table 2).
- 414 II. Type B: (k_1 - k_2) planes are at higher angle ($>25^\circ$) to the dyke plane in case of type
415 B fabric. Multi-domain magnetite particles dominate. Two dykes (10, 46) show
416 this type of fabric. Both of them display oblate susceptibility ellipsoids. Magnetic
417 lineations (k_1) are gently to moderately plunging.
- 418 III. Type C: PSD dominates the grains and the (k_1 - k_2) planes make a high angle with
419 the dyke plane in case of Type C (Anomalous) fabric. Two dykes (SH43, 19)
420 display type C fabric. Both prolate (dyke 19) and oblate (dyke SH43) shape fabric
421 were identified. Magnetic foliation planes are at very high angle to the dyke plane
422 for both dykes striking N-S and NE-SW for dyke 19 and SH43 respectively.
423 Magnetic lineations are gently to moderately plunging (table 2).
- 424 IV. Type D: (k_1 - k_2) planes are oblique to the dyke plane and magnetic lineation is at
425 high angle to the dyke plane. Magnetic grain shows multi-domain status. Three

426 dykes (DND1, 27, 37) show this type of fabric. Magnetic foliation planes strike
427 along WNW-ESE to NW-SE and magnetic lineations show gentle plunge (table
428 2).

429

430 It is to be noted that we have collected multiple samples from more than 45 dykes. Around 30
431 of them failed to display any significant cluster of susceptibility axes and hence, were
432 discarded from interpretation. On closer look, it was identified that majority of them did not
433 observe a significant co-planer relationship between the silicate template and the magnetite
434 template as suggested by Das et al. (2019). The euhedral crystallographic symmetry of the
435 magnetite grains often restricts them to achieve enough shape anisotropy that correlated well
436 with the shape anisotropy of the silicate grains formed by magma flow.

437

438 The degree of confidence for our interpreted flow axes is mainly based on three factors: i)
439 domain structure; ii) corresponding fabric geometry; and iii) significant number of sample
440 (should be more than one) and specimens (multiple specimens from each sample) (Table 2).

441

442 Finally, the distribution of flow axes (trend and plunge) is shown in Fig. 11 and all the
443 obtained flow axes are plotted in the map (Fig. 12). Random distribution of the flow axes
444 throughout DND dyke swarm possibly suggests multi-directional, sub-horizontal to inclined
445 flow of magma within the dykes during their emplacement.

446

447 **5. Discussion:**

448 Interpretation of magma flow direction from AMS data often comes with a number of
449 ambiguities. The first one is to find out, if at all, AMS can be used as a proxy for flow fabric
450 determination. Several researchers have raised their serious concerns about the same

451 (McHone, 2005; Ray et al., 2008). Major criticism comes regarding the late crystallization of
452 ferromagnetic grains in the interstitial spaces of primary silicate framework after the actual
453 flow has stopped. McHone et al. (2005) expressed their strong reservation against using AMS
454 as flow fabric indicators for giant dyke swarms especially for interpreting lateral flow. They
455 argue that AMS is mainly contributed by magnetite grains in basalt, which crystallize when
456 the magma is relatively cold probably after magma flow stopped. As the magma flow fabric
457 should be strongly controlled by plagioclase laths, along whose planar faces the magnetite
458 particles accumulate in layers, flow fabric should be independent of the magnetic fabric.
459 Also, a 3-D plagioclase network (Philpotts & Dickson 2000) subsides and becomes flat in
460 case of sizeable magma body. They also argued that the back-flow after diminishing of the
461 fluid pressure could re-orient both feldspar phenocrysts and surrounding magnetite grains. In
462 two of our publications from recent past (Das et al., 2019a; Das and Mallik, 2020), we have
463 discussed this issue in detail. If the constituent mineral fabric is dominantly governed by the
464 magma flow, then a 'normal' fabric is most likely where k_1 axis and magnetic foliation plane
465 (k_1 - k_2) would reside within or in close proximity to the dyke or intrusion plane. We have also
466 demonstrated this phenomenon in Das et al. (2019a) by analysing the correspondence
467 between 3D SPOs of (Shape Preferred Orientations) the silicate (mainly plagioclase because
468 they crystallise as elongated grains) grains and ferromagnetic grains. Wherever AMS fabric
469 perfectly mimics the orientation of primary fabric governed by silicate mineral (e.g.
470 Plagioclase), AMS fabric shows normal configuration. Where the magnetic fabric does not
471 follow the flow fabric formed by the silicate minerals, the magnetic foliation plane makes
472 oblique or high angle to the dyke plane (i.e. inverse or intermediate fabric). We have also
473 demonstrated (Das and Mallik, 2020) that the margin of a dyke has the best chance to
474 preserve such correspondence because of quick chilling. The centre of a thick dyke mostly

475 provides 'scattered' AMS fabric that is independent of the flow fabric. These findings are
476 supported by earlier group of researchers like Cruden et al. (1996).

477 The second ambiguity comes regarding the definition of 'primary' and 'intermediate/
478 anomalous' fabrics. Cañón-Tapia (2004) genetically suggested that a sample where multi
479 domain (MD) ferromagnetic grains dominate, it should provide primary fabric i.e. the fabric
480 formed due to magma flow. The other definition of primary fabric follows the geometrical
481 configuration of normal fabric i.e. where (k_1-k_2) plane is parallel to the dyke plane and k_1 axis
482 is perpendicular to the dyke axis. Magee et al., (2016) argued that in some cases, where the
483 intrusion got compartmentalized, the primary fabric might not follow the geometrical
484 definition. By the second definition, for all the dykes showing normal fabric, magnetic
485 lineation (k_1) should be along the flow axis! The other interesting problem is that the
486 interpretation of the 'intermediate/ anomalous' fabric is not well discussed in the literature.
487 They are often explained as the effect of alteration, secondary mineralisation etc. (Rochette et
488 al., 1992; Raposo and D'Agrella-Filho, 2000; Raposo and Ernesto, 1995 etc.). Cañón-Tapia
489 (2004) have genetically associated the dominance of pseudo-single domain (PSD) and single
490 domain (SD) grains with intermediate and anomalous fabrics. He suggested that k_3 axis
491 should provide the direction of magma flow axis in case of the dominance of single domain
492 grains. In cases, where pseudo-single domain grains dominate, k_2 is suggested to provide the
493 direction of magma flow axis in very few selected literatures (Khan, 1962). Now with the
494 above, 'genetic' and 'geometrical' definitions in mind following contradictions may often
495 surface due to mixing of geometrically normal and inverse fabric (Ferre, 2002) while
496 interpreting AMS data: a) what if a MD dominated sample does not follow the geometrical
497 definition of primary fabric? And b) what if a SD or PSD grain dominated sample follows the
498 geometrical definition of primary fabric? Magee et al., (2016) discussed that the
499 superimposition of the fabric might be possible due to a) convection within the intrusive, b)

500 inflation or deflation of the late stage intrusions and c) roof collapse due to cessation of
501 magma pressure during the final instant of magma flow etc. According to them, for intrusive
502 sheet thicker than 3m, then the convection could affect or modify the primary flow fabric. In
503 the present article, four of the studied dykes (dyke no. 10, 47, 27 and DND1) with *thickness*
504 $>3m$ show anomalous fabric. However, for two dykes (10 and 46), the k_1 axis is
505 approximately parallel to the dyke plane. This observation indicates that the convection did
506 not affect the flow fabric (Magee et al., 2016).

507 Day's plot (Fig. 8) is used to distinguish the dominant domain structure of the contributing
508 magnetic minerals which is essential to interpret inverse and/or intermediate fabric.
509 Although, the overall angular relationship between the dyke and the susceptibility ellipsoid
510 indicates inclined flow, for the rest of the samples we have followed the following scheme
511 while interpreting the flow direction. If the dyke sample is showing normal fabric, k_1 was
512 assigned as the primary flow axis. In this case, the domain state can be ignored. If the
513 samples display inverse or intermediate fabric then the domain structure is considered. In
514 case of anomalous fabric, they were categorised into two classes. The first category is the one
515 that follows the geometrical definition of anomalous fabric but still dominated by multi-
516 domain (MD) particles. Such anomalous fabric cannot be regarded as the consequence of the
517 magnetic mineralogical complications. If k_1 lies on or very close to the dyke plane, then it can
518 be assigned as primary flow axis (Magee et al., 2016) and for the rest, flow axis can't be
519 interpreted properly as the fabric seem to be altered and magnetic lineation significantly
520 deviates from the dyke plane. For those anomalous fabrics, where PSD grain prevails, flow
521 axis was thought to be parallel to k_2 as per the domain state of the constituent magnetic
522 minerals. We did not have any dyke sample where single domain grains dominated. We also
523 could not have bracketed the intermediate fabrics to be a result of later alterations as no such
524 evidences were recorded from the dykes.

525 This brings to a major conclusion about the flow geometry of the DND dyke swarm that (Fig.
526 11; Table 2), except for few dykes (7, 52, 53, 21), majority of them show signatures of
527 inclined or lateral flow. Moreover, the scattering of resolved flow axes (Fig. 12) indicates the
528 possibility of polycentric flow i.e. kind of flow emerging from several magma sources and no
529 preference is observed in terms of their flow axes orientation. In other words, there were
530 multiple subsurface sources from which magma got emplaced and it flew in all directions
531 perhaps depending on the local topographic slope.

532 Ray et al., (2007), based on field observations (distribution of dyke trend, dyke thickness and
533 length, aspect ratios, crustal dilation etc.) and comparison with other dyke swarms (e.g., Ernst
534 and Duncan, 1995; Ernst et al., 1995; Fialko and Rubin, 1999; Knight and Walker, 1988),
535 made some preliminary assumptions about the flow geometry of DND dyke swarm. They
536 suggested vertical injection from a magma chamber for dykes with a strike dimension smaller
537 than the dip dimension and lateral injection for the rest. Our study, however, does not support
538 such conjecture and we do not observe any relationship between the flow geometry and dyke
539 dimension. Ray et al., (2008) further compared DND dyke swarm with 2,000-kmlong
540 Mackenzie dyke swarm in Canada where vertical magma flow was inferred (based on AMS
541 study) in the central area and that changed to horizontal farther away. Based on the consistent
542 orientation, range in dyke dimension (very long to very short) and comparison with the
543 Iceland dykes (as proposed in Gudmundsson, 1990; 1995a,b), they proposed that both lateral
544 and vertical injections are very much possible for DND dykes. Based on the hypothesis
545 (dykes made up of offset segments are most likely formed by vertical injection and dykes
546 with constant thickness are formed by lateral injection) proposed by Gudmundsson (1990),
547 they suggested that the 79km long Sakri-Dhule-Parola dyke of the DND swarm was probably
548 laterally injected. They also postulated the occurrence of shallow localised magma chambers
549 at the base of the crust similar to Icelandic swarm. Ray et al., (2008) cited the example of two

550 samples of a segmented regional dyke from the DND swarm collected ~35 km apart that
551 showed difference in elemental and Nd–Sr–Pb isotopic compositions (Sheth et al., 1997).
552 Seth et al., (1997) reported their initial $^{87}\text{Sr}/^{86}\text{Sr}$ ratios to be 0.70481 (± 0.00002) and 0.70474,
553 initial ϵNd values to be +1.4 (± 0.2) and +1.5, and present-day $^{206}\text{Pb}/^{204}\text{Pb}$ ratios are 17.483
554 (± 0.012) and 17.578. Ray et al., (2008) suggested that this dyke could be laterally injected
555 because systematic compositional change is expected in case of lateral injection (Greenough
556 and Hodych, 1990, Baragar et al., 1996).

557 Sheth et al., (2019) based on geochemical and isotopic data inferred that Nandurbar-Dhule
558 dykes like NBD10, SDPD2 could have been the feeders to the Jawhar-Igatpuri formation
559 lavas in the Western Ghats. They also suggested that the same dykes fed flows like PL10 and
560 PL11 in the Palitana section (northwesterly extension of the Jawhar Fm). Sheth et al., (2019)
561 further argued that Palitana, Toranmal or Pavagadh lava sections (geographically located in
562 different directions) that shows geochemical signatures of being fed by the DND dyke swarm
563 may not be the products of a single magma chamber or feeder dyke system rather were lava
564 flows originating in “*separate eruptive areas, flowing various distances in different*
565 *directions, and becoming juxtaposed, a scenario of polycentric eruptions*”.

566 The assumptions made by Ray et al., (2008) about the presence of lateral injection are
567 conclusively confirmed by our work. Moreover, we propose that lateral injection is the
568 dominant flow type for DND dyke swarm. Furthermore, the theory proposed by Sheth et al.,
569 (2019) about polycentric eruption is strongly supported by our work. The random sense of
570 primary flow axes implies pouring out of magma from several magma sources and sub-
571 horizontal or inclined flow throughout the dyke swarm. The idea of polycentric flow is
572 further supported by the gravity modelling work by Bhattacharji et al., (2004) where they
573 postulated the presence of up to eight shallow, disconnected fossil magma chambers beneath
574 the dyke swarm. These shallower chambers could have been fed by the large thick mafic

575 magma body which is now preserved as a thick regional igneous intrusive layer at a depth of
576 ~22kms below the Nandurbar-Dhule area (Ray et al., 2008). McHone et al. (2005) and Silver
577 et al. (2006) postulated that such large igneous intrusive layer could be the result of the
578 accumulation of vast pond of magma beneath the lithosphere for several millions of years.
579 During the periods of large crustal extensions (like in case of DND dyke swarm), magma
580 from such ponds can come up to the shallower isolated sub-crustal magma chambers and
581 eventually feed the dyke swarm. The present work and the work by Sheth et al. (2019)
582 provide definitive evidences about lateral flows from this giant dyke swarm. As giant dykes
583 can extend far beyond the radius of the proposed (if at all, one is present) plume heads
584 (McHone, 2005), it will be devoid of sources for vertical flow for such great lengths.

585 Our findings together with the combined knowledge of previous significant works (Ray et al.,
586 2008; Sheth, 2000; Sheth et al., 2019) on DND dyke swarm in a way supports the ‘fissure
587 fed’ theory (Hawkesworth et al., 2000; King and Anderson, 1995; Sheth, 2005; Turner et al.,
588 1996) for Deccan volcanism over the theory of feeding by a large edifice (Duncan and
589 Richards, 1991; Hooper, 1990; Richards et al., 1989; White and McKenzie, 1989) driven
590 volcanism. Sheth (2000) provides a comprehensive list of counter arguments against the
591 theory of post Deccan crustal extension (as proposed by Hooper, 1990). His primary
592 conclusion was that the large Narmada-Satpura-Tapi (DND dyke swarm is a part of this mega
593 dyke swarm) must have fed some flows through vertical injection that are younger than the
594 dykes themselves and immediately above the dyke swarm and must have been eroded by now
595 from the DND area as the rate of erosion of Deccan volcanic rocks could be pretty
596 significant. Now we have categorically suggested the theory of lateral injection and
597 polycentric flow from AMS data, it can very well explain the geochemical similarities
598 between distant flows (like Jawhar-Igatpuri formation, PL10 and PL11 in the Palitana
599 section, Toranmal, Pavagadh flows) and DND dykes. Although, no direct physical field

600 evidence of a feeder dyke is found, geochemical, isotopic and AMS data indirectly proves
601 that the DND dyke swarm was most likely a feeder dyke swarm to some part of the Deccan
602 flood basalt. Hence, we are another step ahead in proving the of 'fissure fed' eruption
603 responsible for Deccan volcanism.

604 Lateral flow in a giant dyke swarm strongly argues for the presence of an associated mantle
605 plume (McHone, 2005). The mantle "plume hypothesis" and the "fissure fed" hypothesis are
606 often presented as 'rivals' in the literature. Pre or syn-deccan crustal extension can be very
607 much due to a combined interplay between mantle plume push and large-scale
608 intercontinental plate dynamics. Already weaker crustal segments along the intercontinental
609 rifts (like the Narmada-Son-Tapi Lineament) could get fractured by the extra push obtained
610 from the mantle plume and form potential conduits (dykes) through which the Deccan lava
611 got emplaced. The emplacement of the deep magma pond as envisaged by McHone et al.,
612 (2005) and Silver et al., (2006), could very well be done by the reunion plume, where the
613 magma lost significant part of its ambient temperature, became more tholeitic and finally got
614 emplaced in batches through the fissures which are preserved as three magnificent dyke
615 swarms. Although, Sheth (2005) provides a number of arguments against the mantle plume
616 origin of Deccan volcanism, it may not be completely discarded at least from the flow
617 geometry of the DND dyke swarm as revealed from the present study.

618 **6. Conclusion:**

619 In this paper, AMS technique is devised to document magma flow pattern to understand
620 magma emplacement mechanisms in and around DND dyke swarm. We discussed the fabric
621 pattern in light of the rock-magnetic aspects. Eventually, compilations of all the data leads to
622 the following conclusions:

- 623 • Titanomagnetite is the main magnetic phase in DND dyke samples. This
624 ferromagnetic mineral is embedded in silicate matrix governed by plagioclase,
625 clinopyroxene etc. No strong evidence in favour of secondary alteration (Like sub-
626 solidus processes, hydrothermal alteration, maghemitization etc.) is observed.
627 Negligible hard-IRM i.e. antiferromagnetic component was detected.
- 628 • Out of fourteen studied dykes, eleven dykes are dominated by multi-domain
629 titanomagnetite. Two third of the rests are showing pseudo-single domain state. For
630 the MD dominated normal fabrics, maximum susceptibility axis (k_1) indicates the flow
631 axis. For anomalous fabrics that are dominated by MD, if the magnetic lineations
632 approximately follow the dyke plane, then the fabric is considered to be not altered
633 due to small scale convection and the magnetic lineation is representative of primary
634 flow axis. In case of PSD dominated anomalous fabric, intermediate susceptibility
635 axis (k_2) represent the flow direction.
- 636 • 28.57% of the studied dykes seem to have experienced vertical/sub-vertical flow,
637 7.14% experienced moderately inclined flow. Gently plunging flow was experienced
638 by 28.57%. Rest 28.57% of the studied dyke shows sub-horizontal flow.
- 639 • Multiple trends of primary flow axes from obtained magnetic fabric support the
640 concept of polycentric flow.
- 641 • Lateral polycentric flow of the DND dyke swarm together with other geochemical
642 evidences provided by earlier researchers provides indirect evidences of the dyke
643 swarm being feeders to the Deccan Flood Basalt supporting the theory of fissure fed
644 volcanism.

645

646 **7. Acknowledgement:**

647 The present work is part of AD's doctoral thesis. JM thanks the financials support provided
648 by SERB under the research grant no ECR/2016/001278. Authors thank IISER Bhopal for
649 providing necessary facilities and infrastructure. Authors thank Mr. Dip Das and Mr.
650 Krishanu Bandyopadhyay for their assistance during field work. Authors thank Prof. Mamilla
651 Venkateshwarlu (NGRI, Hyderabad) and Prof. Satish Sangode (Savitribai Phule Pune
652 University) and their students for extending the rock magnetic lab facilities. The authors thank
653 Dr. V. M. Tiwari, Director, CSIR-National Geophysical Research Institute, for extending support to
654 the Paleomagnetic laboratory facilities. The authors thank Prof. M. G. Kale, HoD, Geology
655 Department, Savitribai Phule Pune University for the permission to conduct the rockmagnetic
656 analysis. All the data produced discussed in this article are available in 4TU.Centre for Research Data
657 (<http://doi.org/10.4121/uuid:59635658-97ce-4cc8-93d9-f1670b8876fa>). Details of the rock
658 magnetic data are available upon request to the author.

659

660 **8. References:**

- 661 1. Alexander, P.O. (1981) Age and duration of Deccan volcanism: K-At evidence, in
662 Deccan Volcanism and Related Flood Basalt Provinces in Other Parts of the World.
663 Edited by K. Subbarao, and R.N. Sukeshwala. Geol. Soc. India Mem. 3, 244-258.
- 664 2. Archanjo, C.J., Trindade, R.I., Macedo, J.W.P. & Araújo, M.G. (2000) Magnetic
665 fabric of a basaltic dyke swarm associated with Mesozoic rifting in north eastern
666 Brazil. *J. S. Am. Earth Sci.*, 13, 179–189.
- 667 3. Baragar, W.R.A., Ernst, R.E., Hulbert, L. & Peterson, T. (1996) Longitudinal
668 petrochemical variations in the Mackenzie dyke swarm, northwestern Canadian shield.
669 *J. Petrol.*, 37, 317–359.
- 670 4. Baer, G. (1995) Fracture propagation and magma flow in segmented dykes: field
671 evidence and fabric analyses. In: Baer, G., Heimann (Eds.), *Physics and Chemistry of*
672 *Dykes*. Makhtesh Ramon, Israel, 125–140.

- 673 5. Baksi, A.K. (1987) Critical evaluation of the Deccan traps, India: Implication for
674 flood-basalt volcanism and faunal extinction. *Geol.* 15, 147-150.
- 675 6. Balasubrahmany, M.N. & Snelling, N.J.E. (1981) Extraneous argon in lavas and dykes
676 of the Deccan volcanic province in Deccan volcanism and related flood basalt
677 provinces in other parts of the world. Edited by K. Subbarao and R. N. Sukeshwala,
678 *Geol. Soc. India Mem.* 3, 259-264.
- 679 7. Beane, J.E., Turner, C.A., Hooper, P.R., Subbarao, K.V. & Walsh, J.N. (1986)
680 Stratigraphy, composition and form of the Deccan basalts, Western Ghats, India.
681 *Bull. Volcanol.*, 48, 61-83.
- 682 8. Bhattacharji, S., Sharma, R. & Chatterjee, N. (2004) Two and three dimensional
683 modelling along western continental margin and intraplate Narmada-Tapti rifts: its
684 relevance to Deccan flood basalt volcanism. In: Sheth HC, Pande K (eds) *Magmatism*
685 *in India through time. Proceeding of the Indian Academy of Science (Earth and*
686 *Planetary Science)*. 113, 771-784.
- 687 9. Bondre, N.R., Duraiswami, R.A. & Dole, G. (2004) Morphology and emplacement of
688 flows from the Deccan Volcanic Province, India. *Bull. Volcanol.*, 66, 29-45.
- 689 10. Brown, R.J., Blake, S., Bondre, N.R., Phadnis, V.M. & Self, S. (2011) Áa lava flows
690 in Deccan Volcanic Province, India and their significance for the nature of continental
691 flood basalt eruptions. *Bull. Volcanol.*, 73(6), 737-752.
- 692 11. Campbell, I.H. (2005) Large igneous provinces and the mantle plume hypothesis.
693 *Elements*, 1(5), 265-269.
- 694 12. Cañón-Tapia, E. (2004) Anisotropy of magnetic susceptibility of lava flows and dykes:
695 a historical account. In: Martin-Hernández, F., Lüneburg, C.M., Aubourg, C., Jackson,
696 M. (Eds.), *Geological Society Special Publications. Magnetic Fabric: Methods and*
697 *Applications*. The Geological Society of London, London, 238, 205-225.

- 698 13. Cañón-Tapia, E. & Chávez-Álvarez, M.J. (2004) Theoretical aspects of particle
699 movement in flowing magma: implications for the anisotropy of magnetic
700 susceptibility of dykes. In: Martin-Hernández, F., Lüneburg, C.M., Aubourg, C.,
701 Jackson, M. (Eds.), Geological Society Special Publications. *Magnetic Fabric:
702 Methods and Applications*, Volume 238. The Geological Society of London, London,
703 227–249.
- 704 14. Cashman, K., Thornber, C. & Kauahikaua, J. (1999) Cooling and crystallization of
705 lava in open channels, and the transition of pahoehoe lava to ‘a’a, *Bull. Volcanol.*, 61,
706 306–323.
- 707 15. Chenet, A.L., Fluteau, F., Courtillot, V., Gérard, M. & Subbarao, K.V. (2008)
708 Determination of rapid Deccan eruptions across the Cretaceous-Tertiary boundary
709 using paleomagnetic secular variation: Results from a 1200-m-thick section in the
710 Mahabaleshwar escarpment. *Jour. Geophys. Res.*, 113(B4), 1-27.
- 711 16. Chenet, A.L., Quidelleur, X., Fluteau, F., Courtillot, V. & Bajpai, S. (2007) $^{40}\text{K}/^{40}\text{Ar}$
712 dating of the Main Deccan large igneous province: Further evidence of KTB age and
713 short duration. *Earth Planet. Sci. Lett.*, 263, 1-15.
- 714 17. Cisowski, S. (1981) Interacting vs. non-interacting single domain behavior in natural
715 and synthetic samples. *Phys. Earth Planet. Int.*, 26, 56–62.
- 716 18. Cox, K.G. & Hawkesworth, C.J. (1985) Geochemical stratigraphy of the Deccan Traps
717 at Mahabaleshwar, Western Ghats, India, with implications for open system magmatic
718 processes. *J. Petrol.*, 26, 355-377.
- 719 19. Courtillot, V., Gallet, Y., Rocchia, R., Féraud, G., Robin, E., Hofmann, C., et al.
720 (2000) Cosmic marker, $^{40}\text{Ar}/^{39}\text{Ar}$ dating and paleomagnetism of the KT section in the
721 Anjar area of the Deccan large igneous province. *Earth Planet. Sc. Lett.*, 182, 137-
722 156.

- 723 20. Courtillot, V., J. Besse, D. Vandamme, R.; Montigny, J. Jaeger, & Cappetta, H. (1986)
724 Deccan flood basalts at the Cretaceous/Tertiary boundary. *Earth Planet. Sc. Lett.*, 80,
725 361-374.
- 726 21. Curtis, M.L., Riley, T.R., Owens, W.H., Leat, P.T. & Duncan., R.A. (2008) The form,
727 distribution and anisotropy of magnetic susceptibility of Jurassic dykes in H.U.
728 Sverdrupfjella, Dronning Maud Land, Antarctica. Implications for dyke swarm
729 emplacement. *J. Struct. Geol.*, 30, 1429–1447.
- 730 22. Cruden, A., Launeau, P. & Tobisch, O.T. (1996) Origin of fabric and compositional
731 patterns in the Dinkey Creek pluton, central Sierra Nevada, California: Emplacement
732 vs post-emplacement flow. In *Geological Society of America Abstracts with Programs*,
733 28, 58).
- 734 23. Dankers, P. (1981) Relationship between medium destructive field and remanent
735 coercive forces for dispersed natural magnetite. *Geophys. J. Roy. Astron. Soc.*, 64, 447–
736 461.
- 737 24. Das, A. & Mallik, J. (2020) Applicability of AMS technique as a flow fabric indicator
738 in dykes: Insight from Nandurbar-Dhule Deccan dyke swarm. *Int. J. Earth Sci.(In*
739 *press)*.
- 740 25. Das, A., Mallik, J. & Bandyopadhyay, K. (2019a) Establishment of correlation
741 between anisotropy of magnetic susceptibility and magma flow fabric: an insight from
742 Nandurbar–Dhule dyke swarm of Deccan Volcanic Province. *Curr. Sci.*, 116, 1468–
743 1471.
- 744 26. Das, A., Mallik, J., Bandyopadhyay, K., & Alam, R. (2019b) A review of Anisotropy
745 of Magnetic Susceptibility analysis of Indian dykes: Implications on magma
746 emplacement. *Iran. J. Earth Sci.*, 11(1).

- 747 27. Day, R., Fuller, M. & Schmidt, V. A. (1977) Hysteresis properties of titanomagnetites:
748 Grain-size and compositional dependence, *Phys. Earth Planet. Inter.*, 13, 260–267.
- 749 28. Deshmukh, S.S. & Sehgal, M.N. (1988) Mafic dyke swarms in Deccan volcanic
750 province of Madhya Pradesh and Maharashtra. *In: K. V. Subbarao (Ed.), Deccan*
751 *Flood Basalts. Mem. Geol. Soc. India*, 10, 323-340.
- 752 29. Dearing, J.A., Bird, P.M., Dann, R.J.L. & Benjamin, S.F. (1997) Secondary
753 ferrimagnetic minerals in Welsh soils: a comparison of mineral magnetic detection
754 methods and implications for mineral formation. *Geophys. J. Int.*, 130, 727– 736.
- 755 30. Devey, C.W. & Lightfoot, P.C. (1986) Volcanological and tectonic control of
756 stratigraphy and structure in the western Deccan Traps. *Bull. Volcanol.*, 48, 195-207.
- 757 31. Dinter, D.A., Carl, B., Bartley, J.M. & Glazner, A.F. (1996) AMS evidence for
758 sinistral shear during emplacement of the Independence dyke swarm, California.
759 *G.S.A. Abstracts with Programs*, 29 (4), A-247.
- 760 32. Duncan, R.A. & Richards, M.A. (1991) Hotspots, mantle plumes, flood basalts, and
761 true polar wander. *Rev. Geophys.*, 29, 31–50.
- 762 33. Dunlop, D. J. & Ö. Özdemir (1997) *Rock Magnetism, Fundamentals and Frontiers*,
763 Cambridge Univ. Press, Cambridge, U. K.
- 764 34. Duraiswami, R.A., Gadpallu, P., Shaikh T.N. & Cardin, N. (2014) Pahoehoe–Aa
765 transitions in the lava flow fields of the western Deccan Traps, India: implications for
766 emplacement dynamics, flood basalt architecture and volcanic stratigraphy. *J. Asian*
767 *Earth Sci.*, 84, 146–166.
- 768 35. Ernst, R.E. (1990) Magma flow directions in two mafic Proterozoic dyke swarms of
769 the Canadian Shield: as estimated using anisotropy of magnetic susceptibility data. *In:*
770 Parker, Rickwood, Tucker (Eds.), *Mafic Dykes and Emplacement Mechanisms*.
771 Balkema, Rotterdam, 231–235.

- 772 36. Ernst, R.E. & Baragar, W.R.A. (1992) Evidence from magnetic fabric for the flow
773 pattern of magma in the Mackenzie giant radiating dyke swarm. *Nature*, 356, 511–513.
- 774 37. Ernst, R.E. & Buchan, K.L. (2003) Recognizing mantle plumes in the geological
775 record. *Annu. Rev. Earth Planet. Sci.*, 31(1), 469–523.
- 776 38. Ernst, R.E. & Duncan, A.R. (1995) Magma Flow in the Giant Botswana Dyke Swarm
777 from Analysis of Magnetic Fabric: *3rd International Dyke Conference Abstracts*.
778 Israel, Jerusalem. 30.
- 779 39. Ernst, R.E., Head, J., Parfitt, E., Grosfils, E. & Wilson, L. (1995) Giant radiating dyke
780 swarm on Earth and Venus. *Earth Sci. Rev.*, 39, 1-58.
- 781 40. Evans, M.E. & Heller, F. (2003) *Environmental Magnetism: Principles and*
782 *Applications of Enviromagnetics*. Academic, San Diego, California. 311p.
- 783 41. Ferre, E.C. (2002) Theoretical models of intermediate and inverse AMS fabrics.
784 *Geophys. Res. Lett.*, 29 (7).
- 785 42. Fialko, Y.A. & Rubin, A.M. (1999) Thermal and mechanical aspects of magma
786 emplacement in giant dike swarms. *Jour. Geophys. Res.*, 104(10), 23033-23049.
- 787 43. Godbole, S.M., Deshmukh, S.S. & Chatterjee, A.K. (1996) Geology and chemical
788 stratigraphy of the basalt flows of Akot – Harisal section from Satpura ranges in the
789 eastern part of the Deccan volcanic province. *Gondwana Geol. Mag. Spec.*, 2, 115-
790 124.
- 791 44. Graham, J.W. (1954) Magnetic anisotropy, an unexploited petrofabric element. *Geol.*
792 *Soc. Am. Bull.*, 65, 1257–1258.
- 793 45. Greenough, J.D. & Hodych, J.P. (1990) Evidence for lateral magma injection in the
794 early Mesozoic dykes of eastern North America. In: Parker AJ, Rickwood PC, Tucker
795 DH (eds) *Mafic dykes and emplacement mechanisms*. Balkema, Rotterdam, 35–46.

- 796 46. Gudmundsson, A. (1990) Dyke emplacement at divergent plate boundaries. In : Parker
797 AJ, Rickwood PC, Tucker DH (eds) *Mafic dykes and emplacement mechanisms*.
798 Balkema, Rotterdam, 47-62.
- 799 47. Gudmundsson, A. (1995a) The geometry and growth of dykes. In : Baer G, Heimann
800 A (eds) *Physics and chemistry of dykes*. Balkema, Rotterdam, 23-34.
- 801 48. Gudmundsson, A. (1995b) Infrastructure and mechanics of volcanic system in Iceland.
802 *J. Volcanol. Geoth. Res.*, 64, 23-34.
- 803 49. Hargraves, R.B., Johnson, D. & Chan, C.Y. (1991) Distribution anisotropy: the cause
804 of AMS in igneous rocks? *Geophys. Res. Lett.*, 18, 2193–2196.
- 805 50. Herrero-Bervera, E., Walker, G.P.L., Canon-Tapia, E. & Garcia, M.O. (2001)
806 Magnetic fabric and inferred flow direction of dikes, conesheets and sill swarm, Isle of
807 Skye, Scotland. *J. Volcanol. Geoth. Res.*, 106, 195-210.
- 808 51. Hawkesworth, C.J., Gallagher, K., Kirstein, L., Mantovani, M., Peate, D. & Turner, S.
809 (2000) Tectonic controls on flood basalt magmatism in the Parana-Etendeka Province.
810 *Earth Planet. Sci. Lett.*, 179, 335–349.
- 811 52. Hrouda, F. (1982) Magnetic anisotropy of rocks and its application in geology and
812 geophysics. *Surv. Geophys.*, 5, 37–82.
- 813 53. Hooper, F. (1990) The timing of crustal extension and the eruption of continental flood
814 basalt. *Letters to nature*. 345, 246-249.
- 815 54. Jay, A.E., Mac Niocaill, C., Widdowson, M., Self, S. & Turner, W. (2009) New
816 palaeomagnetic data from the Mahabaleshwar Plateau, Deccan flood basalt province,
817 India: implications for the volcanostratigraphic architecture of continental flood basalt
818 provinces. *Jour. Geol. Soc. London*, 166, 13-24.

- 819 55. Jay, A.E. & Widdowson, M. (2008) Stratigraphy, structure and volcanology of the SE
820 Deccan continental flood basalt province: implications for eruptive extent and
821 volumes. *Jour. Geol. Soc. London*, 165, 177-188.
- 822 56. Jelinek, V. (1981) Characterization of the magnetic fabric of rocks. *Tectonophysics*,
823 79, T63-T67.
- 824 57. Keller, G., Adatte, T., Bhowmick, P.K., Upadhyay, H., Dave, A., Reddy, A.N. &
825 Jaiprakash, B.C. (2012) Nature and timing of extinctions in Cretaceous-Tertiary
826 planktic foraminifera preserved in Deccan intertrappean sediments of the Krishna–
827 Godavari Basin, India. *Earth Planet. Sci. Lett.*, 341–344, 211–221.
- 828 58. Keller, G., Adatte T., Gardin, S., Bartolini, A. & Bajpai, S. (2008) Main Deccan
829 volcanism phase ends near the K–T boundary: evidence from the Krishna–Godavari
830 Basin, SE India. *Earth Planet. Sci. Lett.*, 268, 293–311.
- 831 59. Keszthelyi, L., Self, S. & Thordarson, T. (1999) Application of recent studies on the
832 emplacement of basaltic lava flows to the Deccan Traps. In: Subbarao, K.V. (ed.)
833 Deccan Volcanic Province. *Mem. Geol. Soc. India*, 43, 485–520.
- 834 60. Khan, M. A (1962) The anisotropy of magnetic susceptibility of some igneous and
835 metamorphic rocks. *Jour. Geophys. Res.*, 67, 2873-2885.
- 836 61. King, S.D. & Anderson, D. (1995) An alternative mechanism of flood basalt
837 formation. *Earth Planet. Sci. Lett.*, 136, 269–279.
- 838 62. Knight, M.D. & Walker, G.P.L. (1988) Magma flow directions in dykes of the Koolao
839 complex, O'ahu, determined from magnetic fabric studies. *Jour. Geophys. Res.*,
840 96(19), 539–544.
- 841 63. Kodama, K.P. (1995) Magnetic Fabrics. *Rev. Geophys.*, Supplement, 1991–1994.

- 842 64. Kumar, A., Parashuramulu, V. & Nagaraju, E. (2015) A 2082 Ma radiating dyke
843 swarm in the Eastern Dharwar Craton, southern India and its implications to Cuddapah
844 basin formation. *Precamb. Res.*, 266, 490-505.
- 845 65. Leonhardt, R. (2006) Analyzing rock magnetic measurements: The RockMagAnalyzer
846 1.0 software. *Comput. Geosci.*, 32(9), 1420-1431.
- 847 66. Liu, Q.S., Roberts, A.P., Larrasoana, J.C., Banerjee, S.K., Guyodo, Y., Tauxe, L. &
848 Frank Oldfield, F. (2012) Environmental Magnetism: Principles and Applications. *Rev.*
849 *Geophys.*, 50, RG4002.
- 850 67. Liu, Q.S., Torrent, J., Maher, B.A., Yu, Y.J., Deng, C.L., Zhu, R.X. & Zhao, X.X.,
851 (2005) Quantifying grain size distribution of pedogenic magnetic particles in Chinese
852 loess and its significance for pedogenesis. *Jour. Geophys. Res.*, 110 (B11102), 1-7.
- 853 68. MacDonald, W.D. & Ellwood, B.B. (1987) Anisotropy of magnetic susceptibility:
854 sedimentological, igneous and structural-tectonic applications. *Rev. Geophys.*, 25,
855 905–909.
- 856 69. Magee, C., O’Driscoll, B., Petronis, M.S. & Stevenson, C.T.E. (2016) Three-
857 dimensional magma flow dynamics within subvolcanic sheet
858 intrusions. *Geosphere*, 12(3), 842-866
- 859 70. Magee, C., Stevenson, C.T.E., Ebmeier, S.K., Keir, D., Hammond, J.O.S. &
860 Gottsmann, J.H. (2018) Magma plumbing systems: a geophysical perspective. *J.*
861 *Petrol.*, 59, 1217–1251.
- 862 71. Mahoney, J.J. (1988) Deccan Traps, In Continental Flood Basalts. Edited by J.D.
863 MacDougall, Kluwer academic, Dordrecht, Netharlands, 151-194.
- 864 72. Mahoney, J.J., Sheth, H.C., Chandrasekharam, D. & Pend, Z.X. (2000) Geochemistry
865 of Flood basalt of the Toranmal Section, Northern Deccan Traps, India: Implications
866 for Regional Deccan Stratigraphy. *J. Petrol.*, 41, 1099-1120.

- 867 73. Martín-Hernández, F., Lüneburg, C.M., Aubourg, C., Jackson, M. & Aubourg, C.,
868 (2004) Magnetic fabric: methods and applications- an introduction, p. 1–7. In: Martín-
869 Hernández, F., Lüneburg, C.M., M., J. (Eds.), *Magnetic Fabric: Methods and*
870 *Applications. Geological Society of London, Sp. Publ., 238-560.*
- 871 74. Martin, S.A., Kavanagh, J.L., Biggin, A.J. & Utley, E.P. (2019) The origin and
872 evolution in mafic sills. *Front. Earth Sci.*, 7, 1-23.
- 873 75. Mathieu, L., van Wyk, de Vries, B., Holohan, E.P., & Troll, V.R. (2008) Dykes, cups,
874 saucers and sills: analogue experiments on magma intrusion into brittle rocks. *Earth*
875 *Planet. Sci. Lett.*, 271, 1–13.
- 876 76. McHone, J.G., Anderson, D.L., Beutel, E.K. & Fialko, Y.A. (2005) Giant dikes, rifts,
877 flood basalts, and plate tectonics; A contention of mantle models. *In: Foulger GR,*
878 *Natlund JH, Presnall DC, and Anderson DL, eds., Plates, Plumes, and Paradigms:*
879 *Geol. Soc. Am.*, Special paper, 388,401-420.
- 880 77. Melusso, L., Sethna, S.F., Morra, V., Khateeb, A. & Javeri, P. (1999) Petrology of the
881 mafic dyke swarm of the Tapti river in the Nandurbar area (Deccan Volcanic
882 province). In: Subbarao KV(ed), Deccan Volcanic province. *Geol. Soc. Ind. Mem.*, 43,
883 735-755.
- 884 78. Ort, M.H., Porreca, M., Geissman, J.W. (2015) The use of palaeomagnetism and rock
885 magnetism to understand volcanic process: introduction, p. 1–11. *In: Ort, M.H.,*
886 *Porreca, M., Geissman, J.W. (Eds.), The Use of Palaeomagnetism and Rock*
887 *Magnetism to Understand Volcanic Process. Geol. Soc. london, Sp. Publ. 396 281 pp.*
- 888 79. Pan, X., Shen, Z., Roberts, P.A., Heslop, D. & Shi, L. (2014) Syntectonic
889 emplacement of Late Cretaceous mafic dyke swarms in coastal southeastern China:
890 Insights from magnetic fabrics, rock magnetism and field evidence. *Tectonophysics*,
891 637, 328–340.

- 892 80. Park, J.K., Tanczyk, E.I. & Desbarats, A. (1988) Magnetic fabric and its significance
893 in the 1400 Ma Mealy diabase dikes of Labrador, Canada. *Jour. Geophys. Res.*, 93,
894 13689–13704.
- 895 81. Patil, S.K. & Arora, B.R. (2003) Palaeomagnetic studies on the dykes of Mumbai
896 region, West coast of Deccan Volcanic Province: Implications on Age and Span of the
897 Deccan Eruptions. *J. Virt. Expl.*, 12, 107-116.
- 898 82. Patil, S.K. & Rao, D.R.K. (2002) Palaeomagnetic and Rock-magnetic studies on the
899 dykes of Goa, west coast of Indian Precambrian Shield. *Phys. Earth Planet. Int.*, 133,
900 111-125.
- 901 83. Paul, D.K., Ray, A., Das, B., Patil, S.K. & Biswas, S.K. (2008) Petrology,
902 geochemistry and paleomagnetism of the earliest magmatic rocks of Deccan Volcanic
903 Province, Kutchh, Northwest India. *Lithos.*, 102, 237-259.
- 904 84. Philpotts, A.R. & Asher, P.M. (1994) Magmatic flow-direction indicators in a giant
905 diabase feeder dyke, Connecticut. *Geology*, 22, 363–366.
- 906 85. Philpotts, A.R. & Dickson, L.D. (2000) The formation of plagioclase chains during
907 convective transfer in basalt magmas. *Nature*, 406, 59-61.
- 908 86. Potter, D.K. & Stephenson, A. (1988) Single-domain particles in rocks and magnetic
909 fabric analysis. *Geophys. Res. Lett.*, 15, 1097–1100.
- 910 87. Prasad, J.N., Patil, S.K., Saraf, P.D., Venkateshwarlu, M. & Rao, D.R.K. (1996)
911 Palaeomagnetism of dyke swarm from the Deccan Volcanic Province of India, *J.*
912 *Geomag, Geoelectr.*, 48, 977-991.
- 913 88. Pratheesh, P., Prasannakumar, V. & Praveen, K. R. (2011) Mafic dykes of Moyar
914 Shear Zone, North Kerala, India: Emplacement history and petrogenetic interpretation
915 based on structure, geochemistry and magnetic fabric. *Iran. J. Earth Sci.*, 3, 185-193.

- 916 89. Putirka, K.D. (2017) Down the crater: where magmas are stored and why they erupt.
917 *Elements*, 13, 11–16.
- 918 90. Raposo, M.I.B. & D'agrella-Filho, M.S. (2000) Magnetic fabrics of dike swarms from
919 SE Bahia State, Brazil: their significance and implications for Mesoproterozoic basic
920 magmatism in the São Francisco Craton. *Precambr. Res.*, 99, 309–325.
- 921 91. Raposo, M.I.B. & Ernesto, M. (1995) Anisotropy of magnetic susceptibility in the
922 Ponta Grossa dyke swarm (Brazil) and its relationship with magma flow direction.
923 *Phys. Earth Planet. Inter.*, 87, 183–196.
- 924 92. Ray, R., Sheth, H.C. & Mallik, J. (2007) Structure and emplacement of the
925 Nandurbar–Dhule mafic dyke swarm, Deccan Traps, and the tectonomagmatic
926 evolution of flood basalts. *Bull. Volcanol.*, 69, 537–551.
- 927 93. Ray, R., Shukla, A.D., Sheth, H.C., Ray, J.S., Duraiswami, R.A., Vanderkluysen, L., et
928 al. (2008) Highly heterogenous Precambrian basement under the central Deccan Traps:
929 Direct evidence from xenoliths in dykes. *Gondwana Res.*, 13, 375–385.
- 930 94. Renne, P.R., Sprain, C.J., Richards, M.A., Self, S., Vanderkluysen, L. & Pande, K.
931 (2015) State shift in Deccan volcanism at the Cretaceous-Paleogene boundary,
932 possibly induced by impact. *Science*, 350(6256), 76-78.
- 933 95. Richards, M.A., Duncan, R.A. & Courtillot, V.E. (1989) Flood basalts and hotspot
934 tracks: plume heads and tails. *Science*, 246, 103–107.
- 935 96. Rochette, P., Jackson, M. & Aubourg, C. (1992) Rock magnetism and the interpretation
936 of anisotropy of magnetic susceptibility. *Rev. Geophys.*, 30, 209–226.
- 937 97. Sharma, P.V. (1994) Late Palaeocene geomagnetic polarity transition in the vestmanna
938 core of the lower basalt sequence on the Faeroe islands. In: Subbarao, K.V. (Ed.),
939 Magnetism: Rocks to Superconductors *Mem. Geol. Soc. India*, No. 10 (supplement).

- 940 98. Schoene, B., Samperton, K.M., Eddy, M.P., Keller, G., Adatte, T., Bowring, S.A., et
941 al. (2015) U-Pb geochronology of the Deccan Traps and relation to the end-Cretaceous
942 mass extinction. *Science*, 347(6218), 182-184.
- 943 99. Sen, G. (2001) Generation of Deccan Trap magmas. Proceedings of the Indian
944 Academy of Science (*Earth and Planetary Science*), 110(4), 409-431.
- 945 100. Sethna, S. F., Khateeb, A., Rao, D. R. K. & Saraf, P. D. (1999) Palaeomagnetic
946 studies of intrusives in the Deccan Trap around Nandurbar Area, South of Tapti Valley,
947 District Dhule, Maharashtra. *Jour. Geol. Soc. Ind.*, 53, 463-470.
- 948 101. Sheth, H.C. (1999a) A historical approach to continental flood basalt volcanism:
949 insights into pre-volcanic rifting, sedimentation, and early alkaline magmatism. *Earth*
950 *planet. Sci. Lett.*, 168(1-2), 19-26.
- 951 102. Sheth, H.C. (1999b) Flood basalts and large igneous provinces from deep mantle
952 plumes: fact, fiction, and fallacy. *Tectonophys.*, 311(1-4), 1-29.
- 953 103. Sheth, H.C. (2000) The timing of crustal extension, dyking, and the eruption of the
954 Deccan flood basalts. *Int. Geol. Rev.*, 42, 1007-1016.
- 955 104. Sheth, H.C. (2005) From Deccan to Reunion: no trace of a mantle plume. In: Foulger,
956 G.R., Natland, J.H., Presnall, D.C., Anderson, D.L. (Eds.), *Plates, Plumes, and*
957 *Paradigm: Geol. Soc. Am. Sp. Pap.*, 388, 477-501.
- 958 105. Sheth, H.C., Duncun, R.A., Chandrashekhar, D., & Mahoney, J.J. (1997) Deccan
959 traps dioritic gabbros from the Western Satpura-Tapi region. *Curr. Sci.*, 72, 755-757.
- 960 106. Sheth, H.C., Mahoney, J.J. & Chandrashekhar, D. (2004) Geochemical
961 Stratigraphy of Deccan flood basalts of Bijasan Ghat Section, Satpura range, India. *J.*
962 *Asian Earth Sci.*, 23, 127-139.
- 963 107. Sheth, H.C., Vanderklyusen, L., Demonerova, E.I., Ivanov, A.V. & Savatenkov,
964 V.M. (2019) Geochemistry and $^{40}\text{Ar}/^{39}\text{Ar}$ geochronology of the Nandurbar-Dhule

- 965 mafic dyke swarm: Dyke-sill-flow correlations and stratigraphic development across
966 the Deccan flood basalt province. *Geol. J.*, 54, 157-176.
- 967 108. Silver, P.G., Behn, M.D., Kelley, K., Schmitz, M. & Savage, B. (2006) Understanding
968 cratonic flood basalts. *Earth. Planet. Sci. Lett.*, 245, 190–201.
- 969 109. Singh, A.P. (1998) 3-D structure and geodynamic evolution of accreted igneous layer
970 in the Narmada-Tapti region (India). *J. Geodyn.*, 25, 129-141.
- 971 110. Speyer, R.F. (1994) *Thermal analysis of materials*. Marcel Dekker, New York.
- 972 111. Staudigel, H., Gee, J., Tauxe, L. & Varga, R.J. (1992) Shallow intrusive directions of
973 sheeted dykes in the Troodos ophiolite: AMS and structural data. *Geology*, 20, 841–
974 844.
- 975 112. Stephenson, A. (1994) Distribution anisotropy: two simple models for magnetic
976 lineation and foliation. *Phys. Earth Planet. Inter.*, 82, 49–53.
- 977 113. Subbarao, K.V. & Hooper, P.R. (1988) Reconnaissance map of the Deccan Basalt
978 Group in the Western Ghats, India. *In*: K.V. Subbarao (Ed.), Deccan Flood Basalts.
979 *Mem. Geol. Soc. India*, 10.
- 980 114. Tarling, D.H. & Hrouda, F. (1993) *The Magnetic Anisotropy of Rocks*. Chapman &
981 Hall, London (217 p).
- 982 115. Thompson, R. & Oldfield, F. (1986) *Environmental Magnetism*. Allen and Unwin,
983 Winchester, Mass.
- 984 116. Tibaldi, A. (2015) Structure of volcano plumbing systems: a review of multi-
985 parametric effects. *J. Volcanol. Geotherm. Res.*, 298, 85-135.
- 986 117. Turner, S., Hawkesworth, C., Gallagher, K., Stewart, K., Peate, D. & Mantovani, M.,
987 (1996) Mantle plumes, flood basalts, and thermal models for melt generation beneath
988 continents: assessment of a conductive heating model and application to the Paraná. *J.*
989 *Geophys. Res.*, 101, 11503–11518.

- 990 118. Vandamme, D. & Courtillot, V. (1992) Paleomagnetic constraints on the structure of
991 the Deccan traps. *Phys. Earth Planet. Inter.*, 74, 241-261.
- 992 119. Venkatachalapathy, R., Loganathan, A., Basavaiah, N. & Manoharan, C. (2009) The
993 use of mineral magnetic parameters to characterize archaeological artifacts. *Lith. J.*
994 *Phys.*, 49(4), 479-485.
- 995 120. Wadia, D. N. (1975) *Geology of India*. New Delhi: Tata McGraw-Hill, 508.
- 996 121. Walker, G. P. L. (1969) Some observations and interpretations on the Deccan Traps.
997 *In: K.V. Subbarao (Ed), 1999, Deccan Volcanic Province. Mem. Geol. Soc. India, 43,*
998 *367–395.*
- 999 122. Walker, G.P.L. (1971) Compound and simple lava flows and flood basalts. *Bull.*
1000 *Volcanol.*, 35, 579-590.
- 1001 123. Wensik, H. (1973) Newer Palaeomagnetic results of the Deccan traps, India.
1002 *Tectonophys.*, 17, 41-59.
- 1003 124. Wensink, H. & Klootwijk, C.T. (1971) Paleomagnetism of the Deccan Traps in the
1004 Western Ghats near Poona (India). *Tectonophys.*, 11, 175-190.
- 1005 125. White, R.S. & McKenzie, D. (1989) Magmatism at rift zones: the generation of
1006 volcanic continental margins and flood basalts. *J. Geophys. Res.*, 94, 7685–7729.

1007
1008
1009
1010
1011
1012
1013
1014
1015
1016
1017
1018
1019
1020
1021

Tables

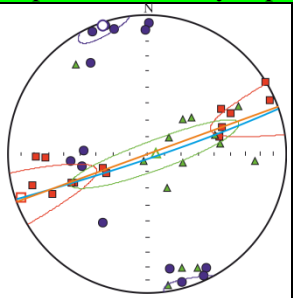
1022
1023
1024
1025
1026

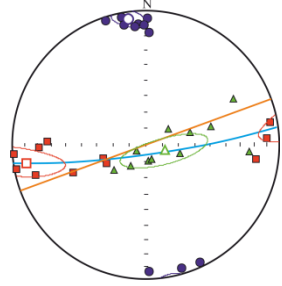
Table 1: Rock magnetic parameters obtained from N-D dyke samples. The units are: $\chi_{lf} = 10^{-8} \text{ m}^3 \text{ kg}^{-1}$, $\chi_{ARM} = 10^{-8} \text{ m}^3 \text{ kg}^{-1}$, and for SIRM, Soft-IRM and HIRM = $10^{-5} \text{ Am}^2 \text{ kg}^{-1}$.

Sample	χ_{lf}	$\chi_{fd}\%$	SIRM	S-Ratio	Soft IRM	Hard IRM
5	114.8735	0.278464	14230.27	-0.9	5708.407	58.64499
7	161.5101	0.576198	13007.51	-0.9	10696.46	257.0643
19	68.48512	0.230924	19530.46	-0.9	3606.096	961.3146
21	187.6472	0.04788	12424.54	-1.0	8647.379	179.0625
27	87.82779	1.318384	10503.89	-0.9	6437.341	520.2843
37	148.0573	0.0943	17676.56	-0.9	8053.071	140.7834
46	156.4772	0.111882	30034.83	-1.0	8038.854	110.0833
52	77.65155	0.085688	19544.32	-0.9	3337.257	929.4582
53	83.91224	0.14617	15086.83	-0.9	5098.37	558.2482
DND1	60.49469	0.782403	10080.94	-0.9	7835.198	88.38967

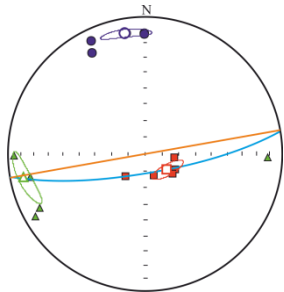
1027

Table 2: Anisotropy of magnetic susceptibility (AMS) data from different sample locations. AMS data are graphically represented in stereonet.

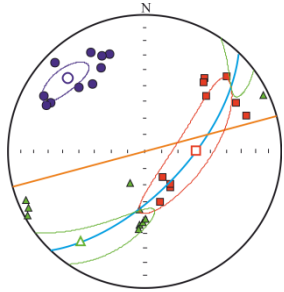
Dyke No	Location (Lat/Long)	Sample No.	Specimens	k _m	T	P	k ₁		k ₂		k ₃		Domain	Geometric definition honoured approximately? (Y/N)	Stereonet	Primary flow axis	Degree of confidence	Remark
							D	I	D	I	D	I						
TYPE A [Geometrical definition: Normal fabric i.e. Magnetic foliation or (k ₁ -k ₂) plane parallel to the dyke plane]																		
5	21.3756° N /74.0838° E	A	a	7	0	1	58.5	0.7	150	66.	328.	23.	MD	Y		4.6°→ 250.8°	High	<ol style="list-style-type: none"> 1) Multi domain grains. 2) Traxial to oblate fabric 3) Magnetic foliation (k₁-k₂) plane parallel to the dyke plane. 4) The pole of magnetic foliation k₃ is better defined than the magnetic lineation k₁ 5) k₁ is assigned as Primary flow axis
			b	2.	.	.	247	27.	46.3	61.	152.	8.7						
			c	3	5	0	248.	43.	83	45.	345.	7.4						
			d	1	0	2	268.	27.	51.3	56.	168.	17.						
			e	0	3	1	66.3	3.9	202.	84.	336	3.7						
		B	a	5	1	1	58.3	37.	156.	10.	259.	50.						
			b	3	5	0	63.6	33.	163.	14.	272.	525						
			c	1	0	2	69.8	42.	320.	19.	212.	41.						
			d	0	3	1	76.7	45.	171	4.1	265	43.						
			e	3	1	1	252.	62.	63	26.	155	3.9						
		C	a	5	1	1	268.	21	105.	68.	0.8	6						
			b	5	4	4	244.	63.	94.5	23.	359.	11.						

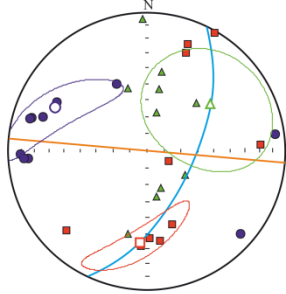
			c				249. 4	41. 8	75.1	48. 1	341. 9	2.8						
			d				254. 9	15. 6	58.1	73. 8	163. 7	4.5						
SD PD 2B	20.944°N/ 74.736°E	SDPD 2B_A	a	7 4.	0 .	1 .	252. 8	60. 7	63	26. 9	155	3.9	MD	Y		10.7° →261. 1°	High	1) Multi domain grains. 2) Traxial to oblate fabric 3) Magnetic foliation (k ₁ -k ₂) plane parallel to the dyke plane. 4) The pole of magnetic foliation k ₃ is better defined than the magnetic lineation k ₁ 5) k ₁ is assigned as Primary flow axis
			b	5 3	2 5	0 3	266. 4	21. 5	105. 9	68. 1	0.8	6						
			c	E -	7 -	0 -	244. 5	62. 8	94.5	23. 4	359. 3	11. 9						
			d	0 3			247. 4	41. 8	75.1	48. 1	341. 9	2.8						
			e				252. 9	15. 6	58.1	73. 8	163. 7	4.5						
		SDPD 2B_B	a				97.2	17. 7	230. 1	64. 9	1.6	17. 2						
			b				266. 1	1	170. 9	79. 3	356. 2	10. 6						
			c				79.6	6.2	230	82. 8	349. 2	3.5						
			d				259. 4	1.7	159. 8	79. 9	349. 7	10						
		SDPD 2B_C	a				272	27. 2	76.2	61. 9	178. 6	6.5						
			b				259. 4	1.7	159. 8	79. 9	349. 7	10						
			c				86.9	10. 2	214. 9	73. 7	354. 6	12. 6						
			d				79.6	6.2	230	82. 8	349. 2	3.5						
7	21.251°N/ 73.989°E	7A	a	3 5.	- 0	1 .	335. 3	71. 4	234. 5	3.6	143. 3	18. 2	MD	Y		79.6° →328. 1°	High	1) Multi domain grains. 2) Prolate fabric 3) Magnetic
			b	5 6	. 1	0 7	337. 6	70. 9	243. 3	1.5	152. 8	19. 1						
			c	E -	1 4	4 4	300. 4	70. 4	72.3	13. 4	165. 7	14. 1						

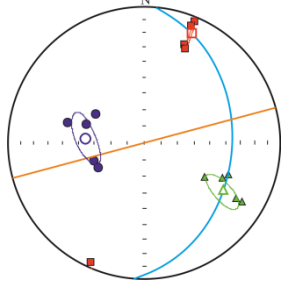
			c	5 E	8 5	3 8	6 121. 2	5 67. 5	239. 8	11. 2	6 333. 7	4 19. 2						2. Oblate fabric 3. Magnetic foliation (k_1 - k_2) plane parallel to the dyke plane. 4. Minimum susceptibility axis k_3 is clustered around the pole of the dyke plane. 5. k_1 is assigned as Primary flow axis
		52B	d	0			177	79. 4	59	5.1	328. 2	9.3						
			e	3			165. 6	79. 6	47.2	5	316. 4	9.1						
			a				124. 8	48. 1	334. 7	37. 9	232. 5	15. 2						
			b				108. 5	40. 6	288. 2	49. 4	18.3	0.1						
			c				130. 6	39. 4	348. 7	43. 7	238. 1	20. 2						
53	21.303°N/ 74.053°E	53A	a	2 4.	0 .	1 .	335. 3	71. 4	234. 5	3.6	143. 3	18. 2	MD	Y		80.7° →326. 1°	High	1. Multi domain grains. 2. Traxial to oblate fabric 3. Magnetic foliation (k_1 - k_2) plane parallel to the dyke plane. 4. The magnetic lineation k_1 well clustered and steeply plunging. 5. k_1 is assigned as Primary flow
			b	6 6	1 3	0 4	337. 6	70. 9	243. 3	1.5	152. 8	19. 1						
			c	E	2	5	300. 4	70. 4	72.3	13. 4	165. 7	14. 1						
			d	0			323. 3	70. 8	71.4	6.2	163. 5	18. 1						
			e	3			309. 6	69. 6	69.6	10. 5	162. 9	17. 2						
		53B	a				330. 8	88. 2	91.4	0.9	181. 5	1.5						
			b				323. 5	86. 4	92.9	2.3	183	2.8						
			c				355. 1	82. 9	88.4	0.4	178. 5	7.1						
			d				314. 3	87. 3	90.1	2	180. 2	1.9						

																	axis	
21	21.289°N/ 74.361°E		a	3 9.	- 0	1 .	159. 0	76. 5	268. 5	4.6	359. 5	12. 7	MD	Y		74.4° →126. 4°	Mediu m	<ol style="list-style-type: none"> 1. Multi domain grains. 2. Prolate fabric 3. Magnetic foliation (k_1-k_2) plane parallel to the dyke plane. 4. The magnetic lineation k_1 well clustered and steeply plunging. 5. k_1 is assigned as Primary flow axis
			b	7 9	.	0 3	220. 8	72. 4	92.1	11. 2	359. 4	13. 4						
			c	E - 0	9 4	7	117. 7	70. 1	257. 8	15. 6	351. 3	12. 2						
			d	0 3			126 2	70. 2	239. 6	8.2	332. 3	17. 9						
			e				96.4	72. 7	242. 1	14. 4	334. 5	9.3						

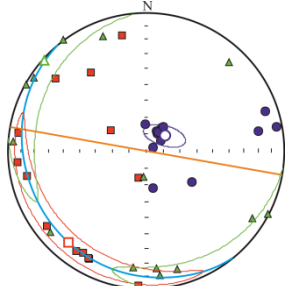
TYPE B [Geometrical definition: Anomalous fabric i.e. Magnetic foliation or (k_1 - k_2) plane oblique to the dyke plane, Magnetic lineation (k_1) approximately parallels the dyke plane; Domain: MD]

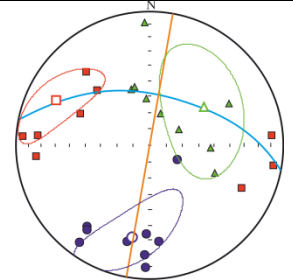
46	21.265°N/ 74.237°E	A	a	4 2.	0 .	1 .	257. 6	7.4	155. 1	59. 2	351. 9	29. 7	MD	Y		59°→8 9.1°	Mediu m	<ol style="list-style-type: none"> 1) Multi-domain particles 2) Oblate fabric 3) Magnetic foliation plane (k_1-k_2) intersect the dyke plane at angle $> 25^\circ$.
			b	0 1	4 9	0 1	144 7	63. 7	247. 1	6.4	340. 1	25. 4						
			c	E - 0	2 3	1	145 3	71. 3	240. 8	2	331. 4	18. 6						
			d	0 3			141. 9	65. 1	243. 6	5.4	336	24. 2						
			e				163. 3	58. 2	65.3	4.9	332. 4	31. 3						
		B	a				70.7	22	183. 7	44. 1	322. 5	37. 8						

																		control. 6) k_1 is assigned as the Primary flow axis.
TYPE C [Geometrical definition: Anomalous fabric i.e. Magnetic foliation or (k_1-k_2) plane being largely perpendicular to the dyke plane; domain: PSD]																		
19	21.3774° N/74.3654°E	19A	a	4 4.	0 .	1 .	178. 4	36. 9	342. 5	52	82.5	7.7	PSD	Y		43.3° →54.6°	High	1) Pseudo single domain particles 2) Oblate fabric 3) Magnetic foliation plane (k_1 - k_2) at high angle to the trend of the dyke. 4) Geometrical pattern is justified by domain structure (PSD). 5) k_2 is assigned as Primary flow axis acknowledging the domain state.
			b	6 3	3 0	0 0	183. 6	31. 9	46.5	49. 7	288. 2	22						
			c	E -	4 4	6 6	161. 3	43. 5	10.7	42. 6	266. 2	15. 2						
			d	0 3			171. 8	34. 9	11.2	53. 5	268. 4	9.3						
			e				115. 9	76. 2	358. 0	6.6	266. 5	12. 1						
		19B	a				29.7	2.4	124. 3	62. 9	298. 5	27						
			b				87.1	19. 4	192. 7	37. 5	335. 6	46. 1						
			c				20.9	18. 7	160. 6	66	285. 9	14. 4						
			d				225. 6	19. 3	14.6	67. 7	131. 8	10. 6						
			e				21.7	24. 8	168. 9	61. 3	285. 2	13. 7						
SH 43	21.489°N/ 74.491°E		a	2 5.	- 0.	1 .	22.5	3.4	115	36. 6	287. 9	53. 2	PSD	Y		32.4° →121. 7°	High	1) PSD particles 2) Prolate
			b	9 9	. 0	0 1	204. 1	4.4	111. 1	33. 9	300. 6	55. 7						

			c	E	6	4	22.1	22.7	121.7	21.7	250.8	57.7						<p>fabric</p> <p>3) (k_1-k_2) plane at high angle to the dyke plane.</p> <p>4) Geometrical pattern is justified by domain structure (PSD).</p> <p>5) k_2 is assigned as the Primary flow axis acknowledging the domain state.</p>
			d	0			21.7	7.7	120.2	47.6	284.9	41.4						
			e	3			23.5	25.6	121.8	16.8	241.6	58.7						

TYPE D: UNRESOLVED Geometrical definition: Anomalous fabric i.e. Magnetic foliation or (k_1 - k_2) plane oblique to the dyke plane, Magnetic lineation (k_1) largely deviates from the dyke plane; Domain: MD

27	21.0581° N/74.3546 °E	27A	a	2	0	1	207.8	13	117.8	0	27.7	77	MD	Y				<p>1) Multi-domain particles</p> <p>2) Oblate fabric.</p> <p>3) Magnetic foliation plane (k_1-k_2) intersect the dyke plane at high angle</p> <p>4) Very gently plunging</p>
			b	6	.	.	211.8	14.4	302.7	3.6	46.3	75.2						
			c	7	8	0	233	10.6	323.1	0.6	56.6	79.4						
			d	0	E	0	208.3	13.1	298.5	0.9	32.4	76.8						
			e	3			258.2	13	165.6	11.3	36	72.6						
		27B	a				214.8	12.8	122.7	9.1	358.2	74.2						
			b				264.9	7.3	173.7	9.4	32.2	78.1						
			c				278.	7.1	186.	14.	32.9	73.						

			d				2		3	8		5					(20°) magnetic lineation (k ₁)		
		27C	a				183. 3	2.5	273. 5	4.1	62	85. 3							
			b				197. 1	73. 6	339. 2	13	71.5	9.7							
			c				348. 1	15. 5	185	73. 8	79.3	4.5							
							300. 7	65. 9	175. 1	14. 6	80.0	18. 7							
DN D1	20.878°N/ 74.570°E	DND1 _A	a	1 6.	- 0	1 .	323. 5	86. 4	92.9	2.3	183	2.8	MD	Y		1) Multi-domain particles 2) Magnetic foliation plane (k ₁ -k ₂) intersect the dyke plane almost perpendicularly 3) Gently plunging (20°-30°) Magnetic lineation (k ₁) 4) When the k ₃ axes are off-vertically clustered, they also can be a flow indicator that can be produced by inclined grain rolling in high energy			
			b	3 2	2 2	355. 1	82. 9	88.4	0.4	178. 5	7.1								
			c	E 4	- 8	3	314. 3	87. 3	90.1	2	180. 2	1.9							
			d	0		3	294. 7	42. 6	62.9	33. 9	174. 5	28. 7							
			e	3			319. 4	28. 1	93.5	52. 5	216. 6	22. 7							
		DND1 _B	a				99.4	7.2	355. 6	62. 1	193. 1	26. 8							
			b				274. 3	5.4	19.4	70. 2	182. 4	19							
			c				274. 9	17. 2	64	70. 2	181. 9	9.6							
			d				264. 7	15. 8	357. 5	9.7	117. 8	71. 3							

Figures

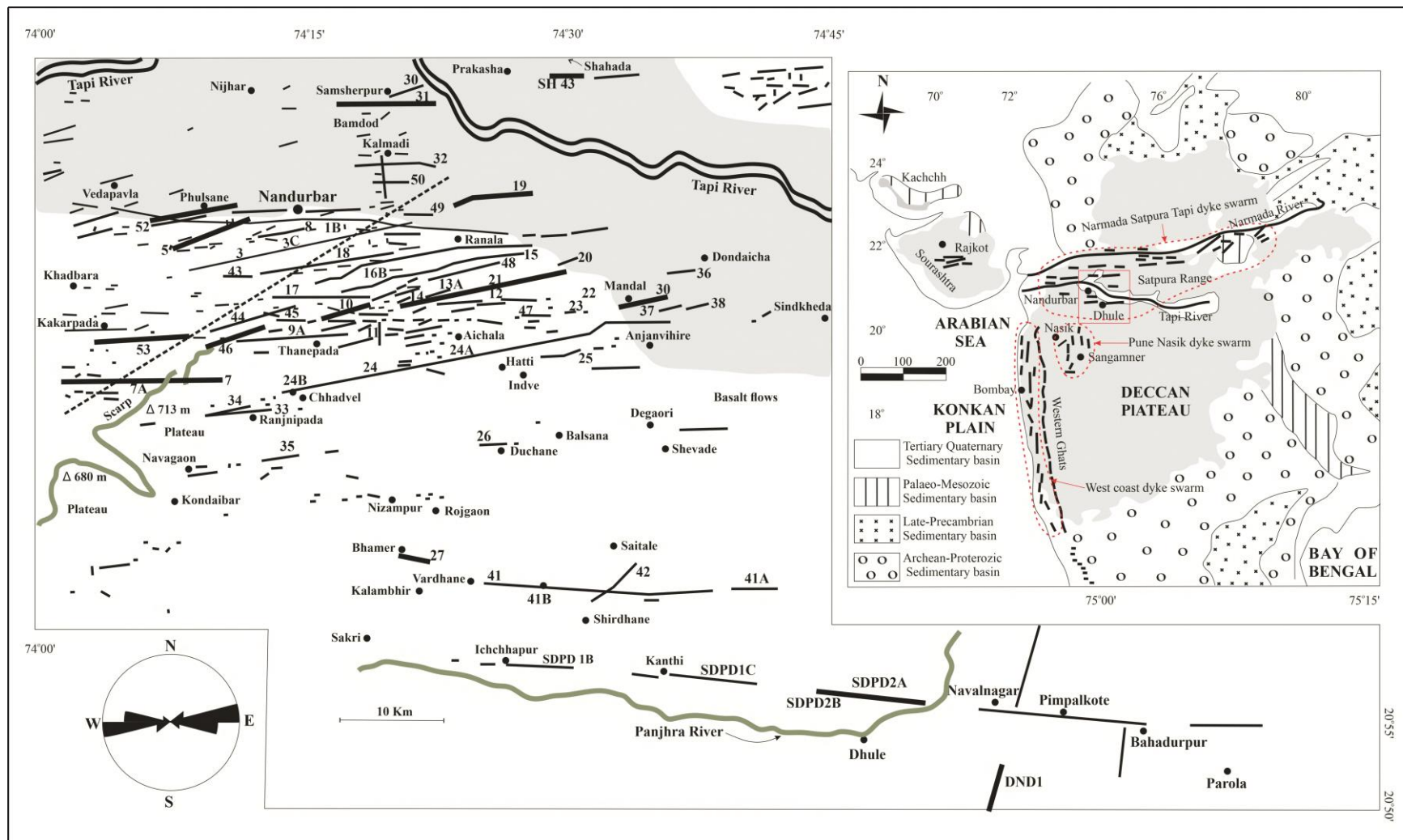


Fig. 1: Regional map of Nandurbar-Dhule Deccan dyke Swarm showing the distribution of dykes (Modified after Ray et al., 2007). Top right inset shows a key map of Western India highlighting the extent of Deccan Flood Basalt Province (shaded). Bottom left inset shows the angular distribution of dyke trends. The studied dykes are shown in bold.

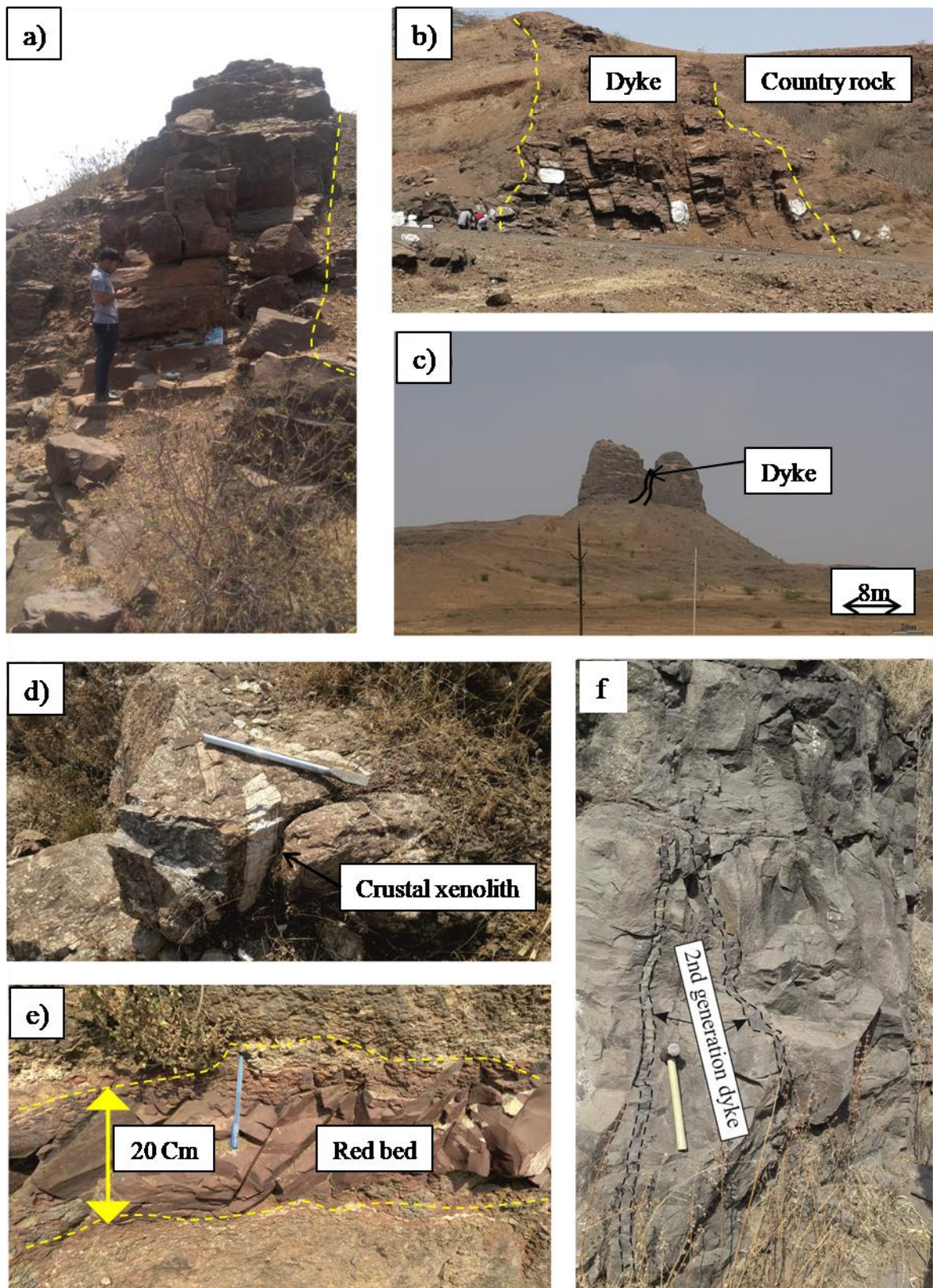


Fig. 2: Field photographs from different dykes: (a) and (b) Dykes standing out like ridge and intruding weathered Deccan flood basaltd near Vardhane ; (c) Dyke cutting through elevated flood basalt pile; (d) Crustal xenolith trapped within a dyke near Rajmane; (e) Occurrence of

red bed within basaltic country rock near chhadvel. See Fig. 1 for the locations; (f) Very thin, relatively fresh second generation dykes cutting through larger dykes.

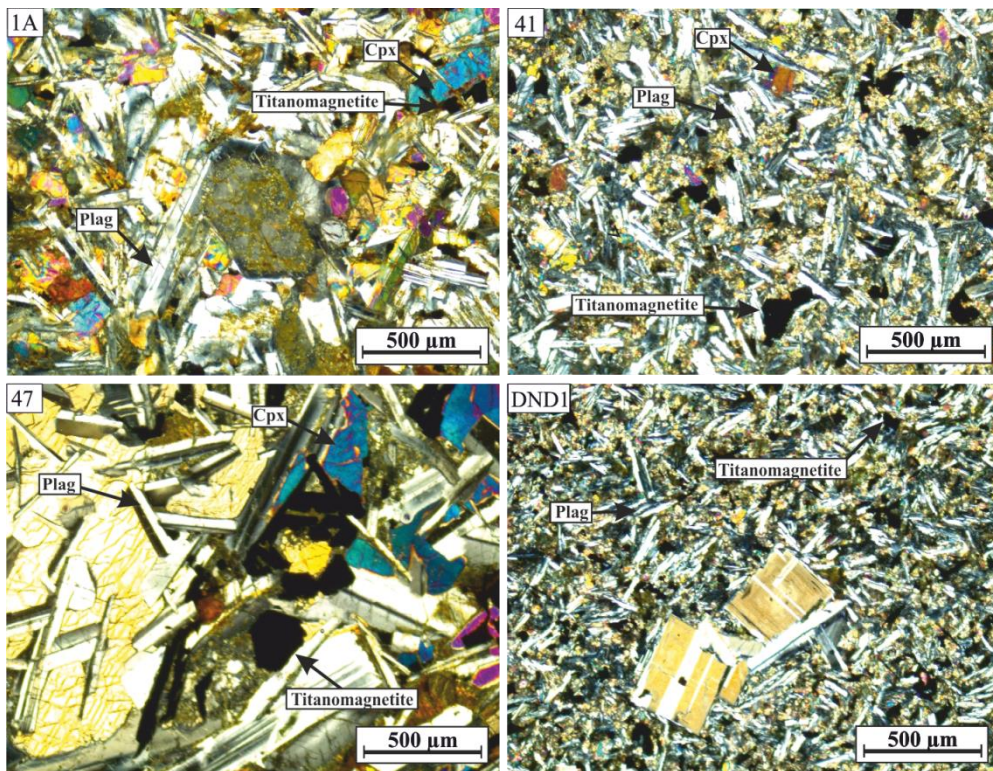


Fig.3: Transmitted light photomicrograph showing mutual occurrence of plagioclase (Plag), clinopyroxene (Cpx) and opaque (Titanomagnetite). All sections exhibit ophitic to sub-ophitic texture.

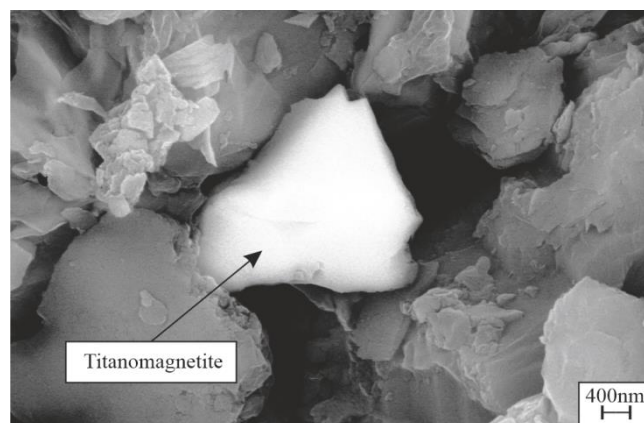


Fig. 4: Scanning Electron Microscopic photograph from dyke sample showing white coloured Titanomagnetites embedded in the dark coloured silicate matrix.

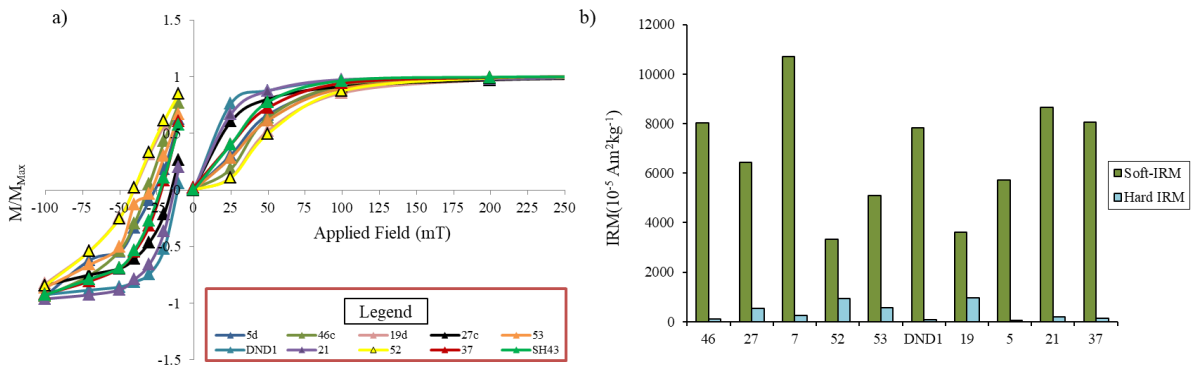


Fig. 5: a) Isothermal Remanence Magnetisation (IRM) acquisition and back-field curves normalized over max IRM value i.e. M_{max} . b) Sample wise estimated soft and Hard-IRM content showing the dominance of soft ferromagnetic phases.

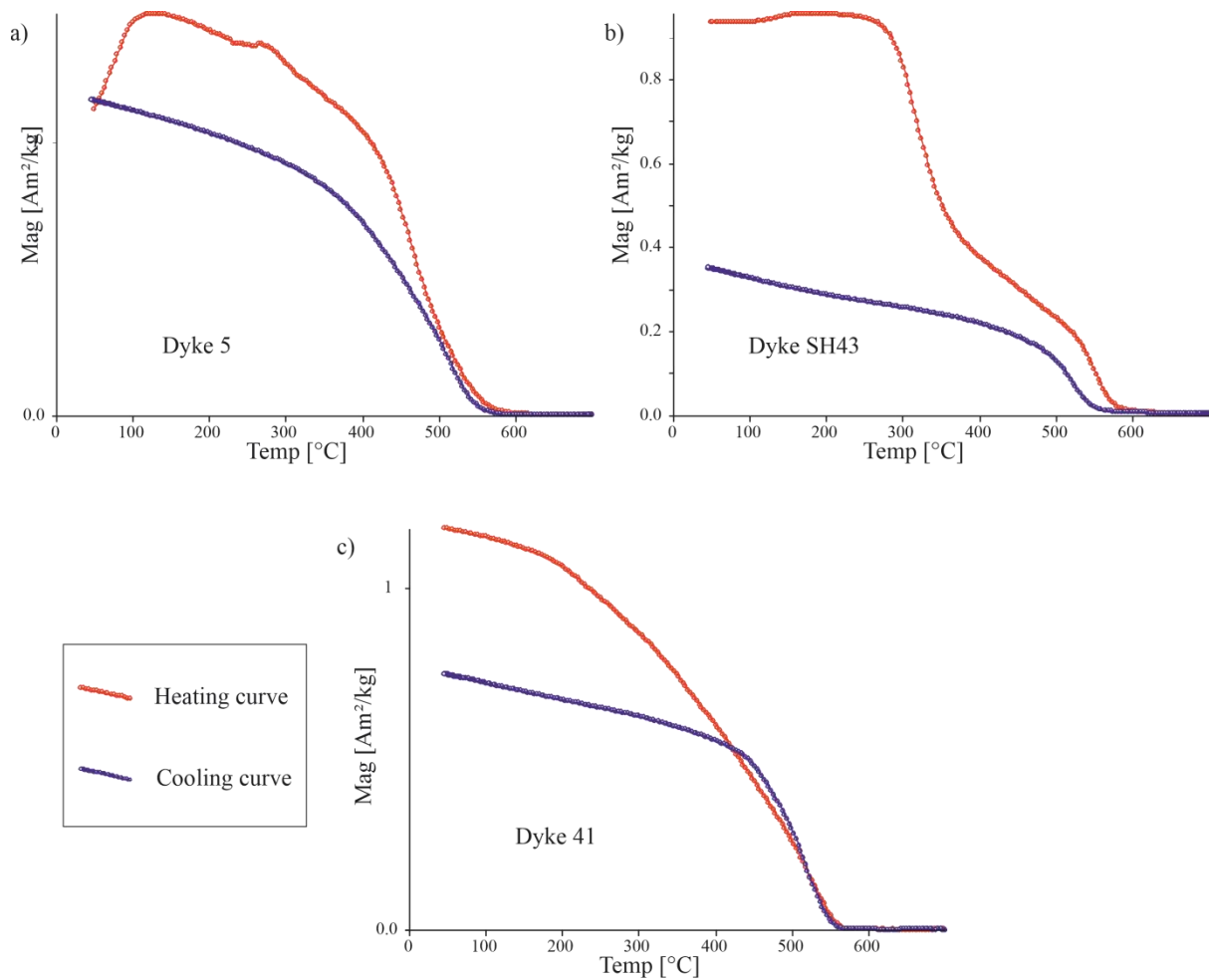


Fig. 6: Temperature dependant susceptibility curves for three representative dyke samples. All the samples show approximately similar Curie temperature ($\sim 570^{\circ}C$) implying Titanomagnetite as the major remanent carrier.

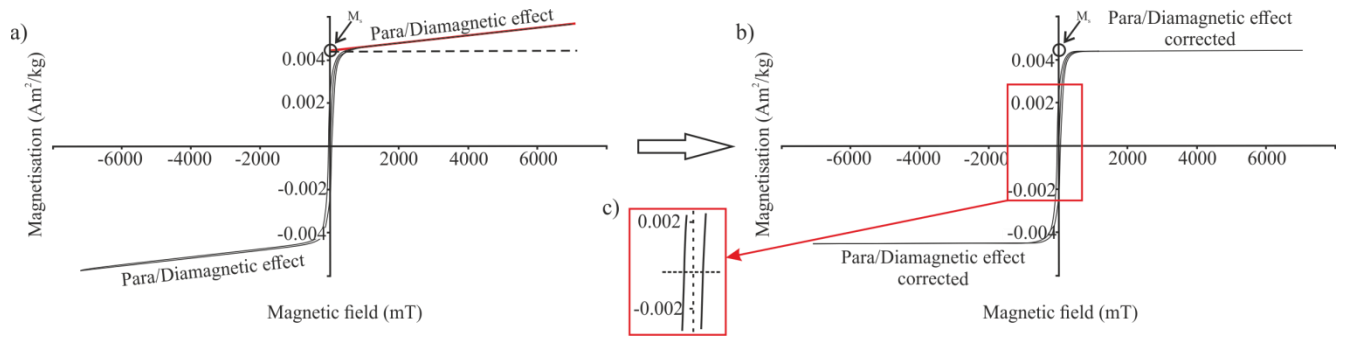


Fig. 7: Hysteresis loop for one representative dyke sample: a) Hysteresis loop including para and dia-magnetic influence. b) Hysteresis loop after para and dia-magnetic correction; c) inset showing zoomed in portion of the loop.

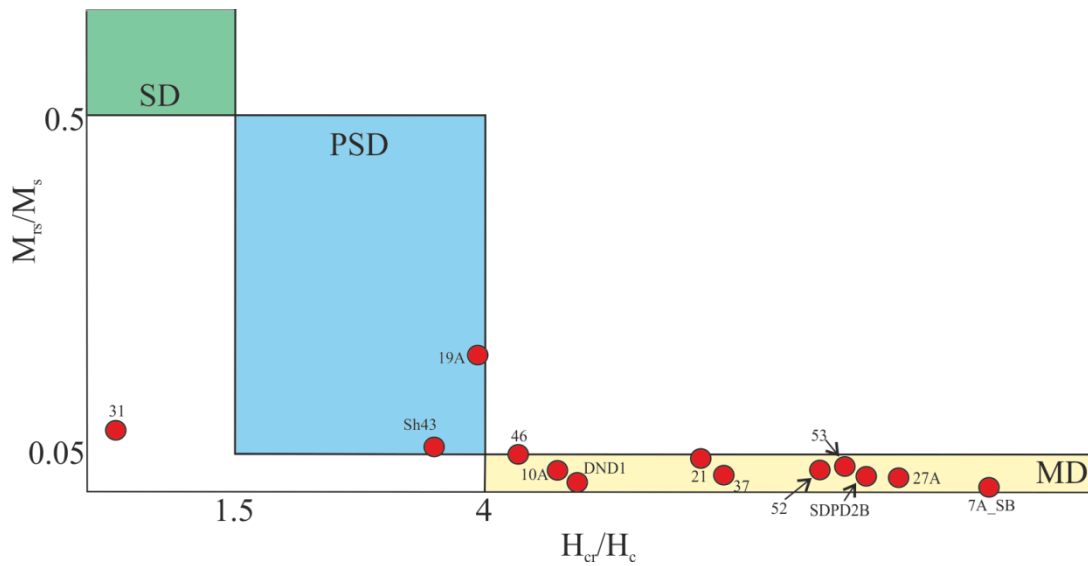


Fig. 8: Hysteresis parameters computed from obtained hysteresis loop after removal of para/dia-magnetic effect. The parameters are plotted on a Day coordinate frame (Day *et al.*, 1977.).

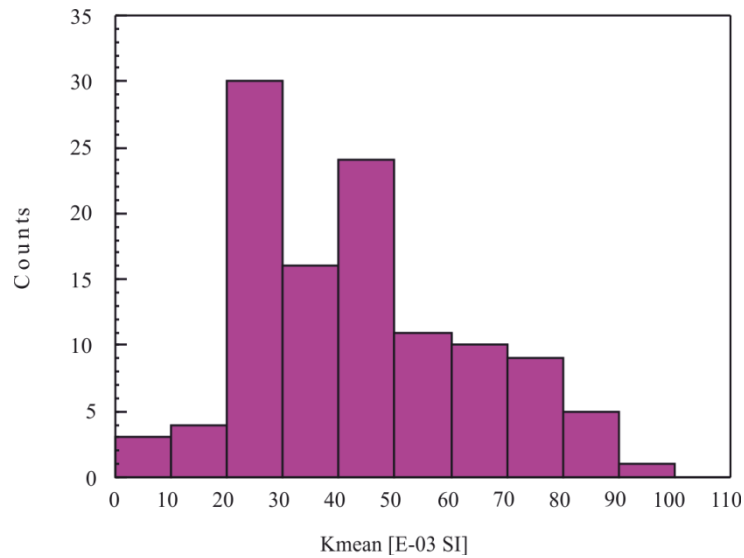


Fig. 9: Histogram showing distribution of the mean susceptibility of different samples.

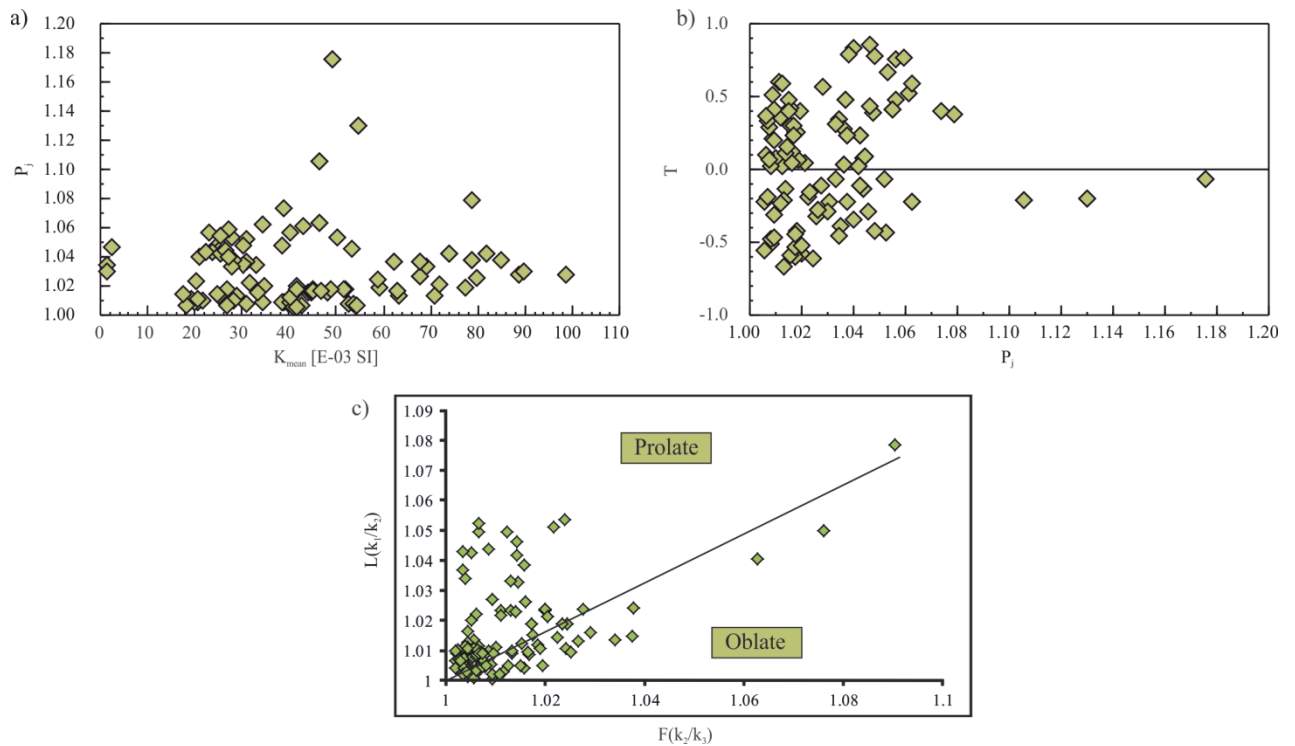


Fig. 10: a) The mean susceptibility (K_m) Vs. degree of anisotropy (P_j) bivariate plot for DND dyke samples showing low and constricted range for P_j except a few outliers. b) Jelinek plot (P_j versus T ; Tarling and Hrouda 1993) manifests the occurrence of both oblate and prolate fabric. c) Magnetic lineation (L) Vs. magnetic foliation (k_1-k_2) plot shows the occurrence of both lineation and foliation.

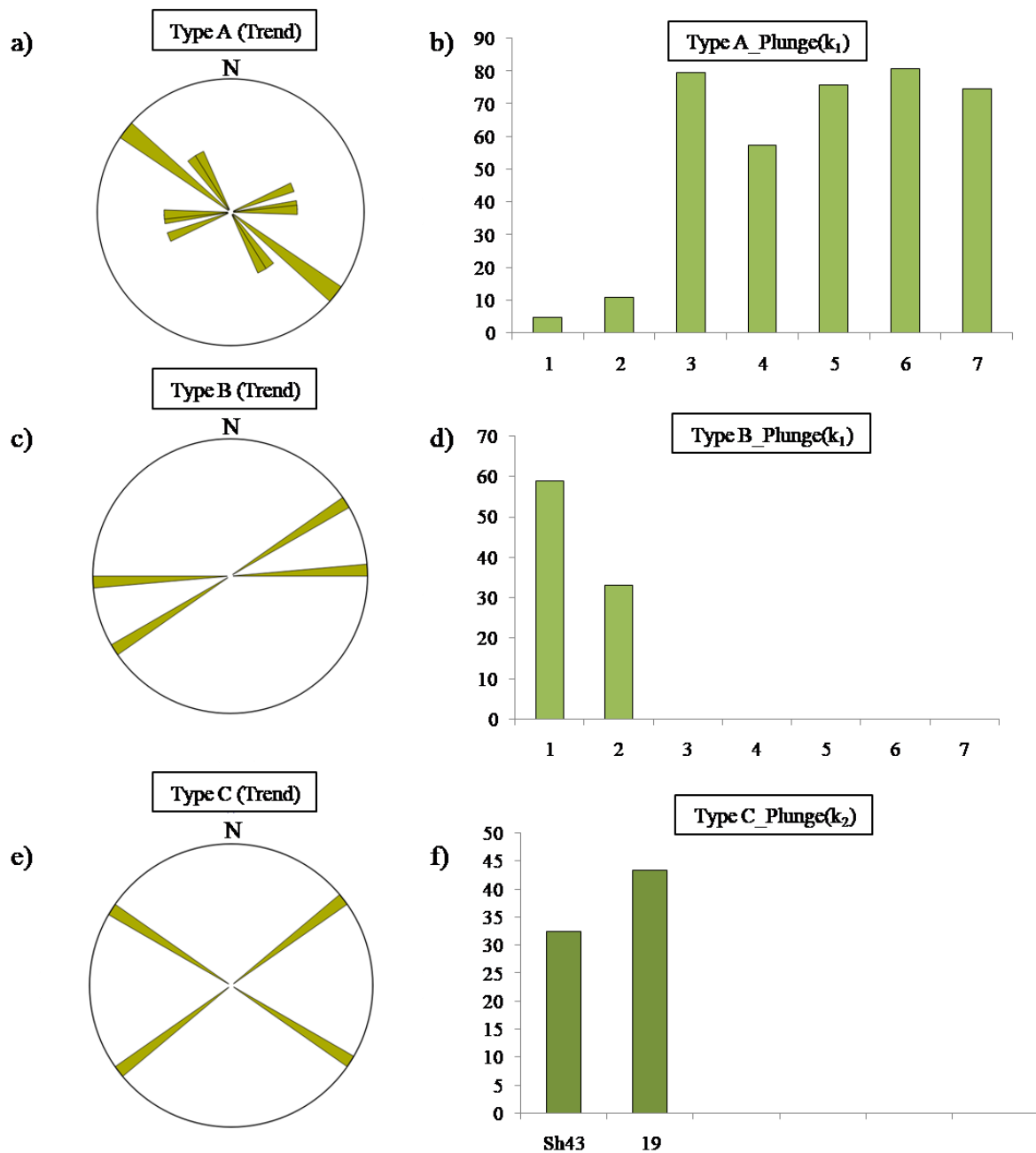


Fig. 11: Rose diagram and bar chart showing the flow direction variation for different type of fabric: a), c) and d) represent the distribution of the trend of the flow using the rose diagram for Type A, B and C fabric; b), d) and f) exhibit the variation of inclination of the flow directions within the dykes for the corresponding fabric type.

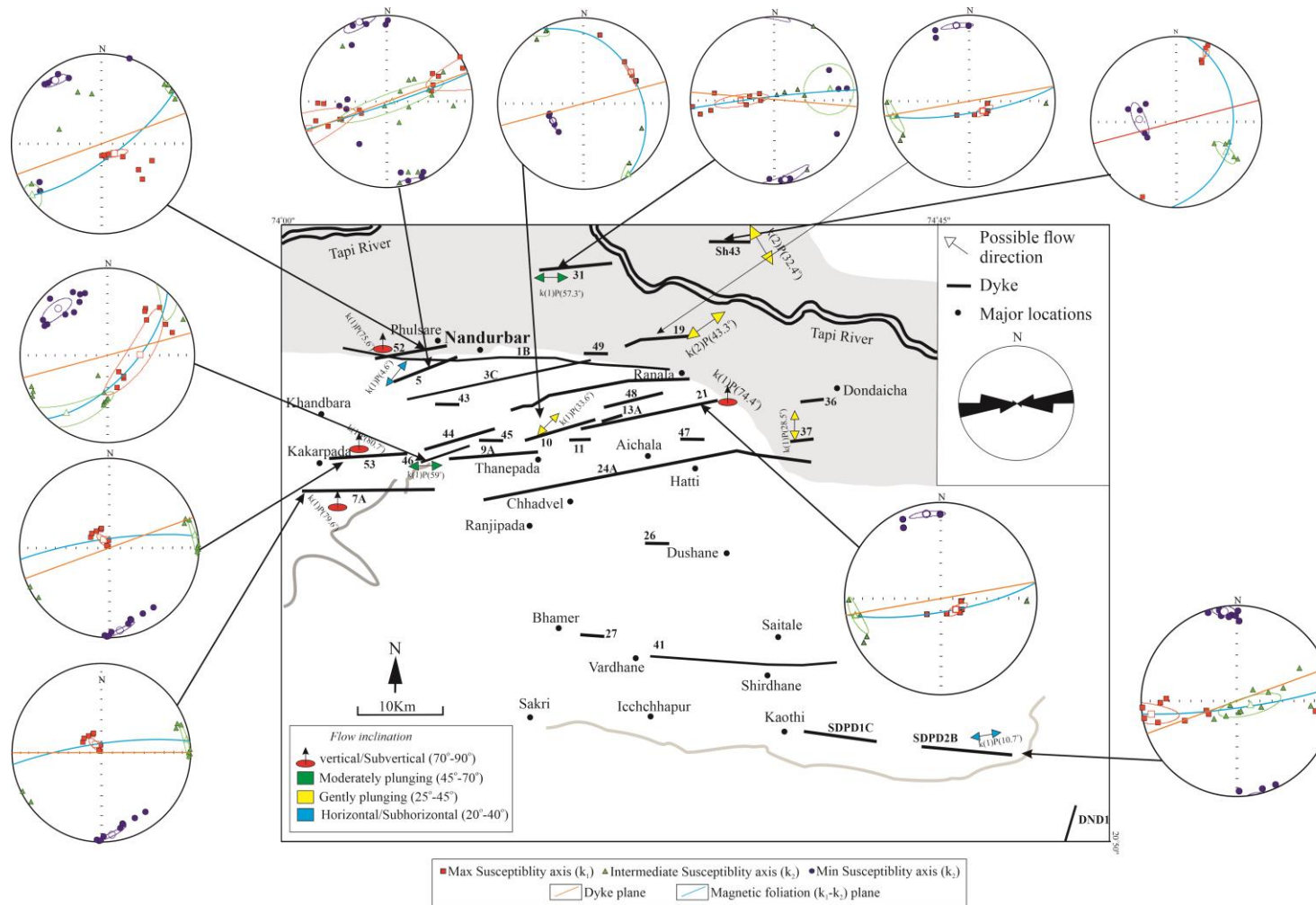


Fig. 12: Map of DND dyke swarm with interpretable dykes and inferred flow direction. Trend of the primary flow axes are exhibited by double headed arrow with different color index depending upon the plunge. Note the absence of any unique pattern of magma flow across the study area.

